



Impact of carbon chain length on the adsorption kinetics of bis-mercapto-benzimidazole MB-C_n-MB ($n = 2, 4, 6, 8, 10$) at the Q235-steel/1 M HCl interface

N. Achnine,¹ M. Driouch,¹ * W. Niouri,¹ M. Kadiri,¹ E.H. El Assiri,¹ A. Mousaif,² A. Haoudi,³ A. Mazzah,⁴ M. Sfaira,¹ S. Kaya,⁵ L. Guo⁶ and A. Zarrouk⁷ **

¹Laboratory of Engineering, Modeling and Systems Analysis (LIMAS), Faculty of Sciences, Sidi Mohamed Ben Abdellah University (USMBA), P.O. Box 1796-30000, Fez-Atlas, Morocco

²Maâmoura National Centre for Energy, Science and Nuclear Technology, “CNESTEN”, Biotechnology and Biomolecule Engineering Unit, Life Sciences Division, Scientific Studies and Research Department, B.P. 1382, Rabat, Morocco

³Laboratory of Applied Organic Chemistry, Faculty of Sciences and Techniques, Sidi Mohamed Ben Abdellah University, B.P. 2202, Route d'Imouzzer, Fez 30050, Morocco

⁴University of Lille, CNRS, USR 3290, MSAP, Miniaturization for Synthesis, Analysis and Proteomics, Lille, France

⁵Department of Chemistry, Faculty of Science, Cumhuriyet University, Sivas 58140, Turkey

⁶School of Material and Chemical Engineering, Tongren University, Tongren, 554300, China

⁷Laboratory of Materials, Nanotechnology and Environment, Faculty of Sciences, Mohammed V University in Rabat, Av. Ibn Battouta, P.O. Box. 1014, Agdal-Rabat, Morocco

E-mail: *majid.driouch.usmba@gmail.com; **azarrouk@gmail.com

Abstract

In the present work, we undertook a study on the effect of increasing the carbon chain from two to ten atoms on bolaform surfactants whose head was a mercapto-benzimidazole {MB-C_n-MB with $n = 2, 4, 6, 8$ & 10 }. A comparative study of the inhibiting effect of MB-C₂-MB and MB-C₈-MB at different concentrations was carried out by comparing three techniques, direct (gravimetric) and indirect (stationary {potentiodynamic polarization, PDP} and transient {electrochemical impedance spectroscopy, EIS}). The polarization curves were analyzed qualitatively by visual inspection and then quantitatively by fitting their data using three methods {Tafel-Fit, Stern-Fit or Wagner & Traud-Fit, and Jena & Bonhoeffer-Fit} while those from the transient method were examined both by graphical inspection of Nyquist, Bode and Betova representations, then modeled and fitted using an appropriate equivalent electrical circuit, EEC. To overcome some ambiguities inherent to basic approximations of Tafel's

method, discussed in this paper, the cathodic and anodic polarization curves were recorded separately with a potential sweep from low to high overvoltage, then adjusted using the Stern and Jena–Bonhoeffer model. Indeed, examination of the results showed that the approximations inherent in the Tafel treatment and the fitting procedure undertaken led to an overestimation of i_{corr} value compared with its value estimated using the Stern model at each concentration of MB-C₂-MB and MB-C₈-MB. Also, we have exhaustively examined the ambiguities, little discussed in the contemporary literature, associated with the modeling, quantitative, and qualitative interpretation of impedance data containing more than one indistinguishable time constant. The inhibiting efficiencies derived from different techniques and methods undertaken showed that MB-C₈-MB was more effective than MB-C₂-MB. To develop an insight into the inhibition mechanism of MB-C₈-MB, six adsorption isotherms, commonly used in the literature, were adapted to the experimental data and critically discussed. The Langmuir model was discarded despite the good statistical parameters of fit, because it remains a hypothetical model that can in no way reproduce the reality of the studied interface. Finally, the polarization resistance values obtained from EIS results for the optimum concentration of 10^{-3} M of the different surfactants studied showed that the inhibition efficiencies followed the trend $\{ \eta\%(\text{MB-C}_2\text{-MB}) = 84\% < \eta\%(\text{MB-C}_4\text{-MB}) < \eta\%(\text{MB-C}_6\text{-MB}) < \eta\%(\text{MB-C}_8\text{-MB}) \approx \eta\%(\text{MB-C}_{10}\text{-MB}) = 96\% \}$.

Received: November 27, 2023. Published: December 22, 2023 doi: [10.17675/2305-6894-2023-12-4-53](https://doi.org/10.17675/2305-6894-2023-12-4-53)

Keywords: Q235-steel, acid corrosion, bis-mercaptobenzimidazole, Tafel, Wagner–Traud, Stern–Geary & Jena–Bonhoeffer models, EIS, EEC, isotherm models.

1. Introduction

The low cost of Q235-steel makes it an attractive choice and a preferred option in various fields of large-scale construction and engineering, where the quantity of steel required is quite significant. In fact, Q235-steel has mechanical properties suitable for many industrial applications. It offers the right combination of mechanical strength, ductility and formability, making it adaptable to a variety of design requirements. However, due to its predominantly carbon-based composition, Q235-steel can be susceptible to corrosion, especially in corrosive environments such as acidic media [1–3].

Although hydrochloric acid (HCl) is particularly aggressive towards metals, including steel, it is frequently used in pickling baths to remove oxides, impurities, welding residues and metal coatings [4–7]. However, due to its corrosive nature and potential risks to health and the environment, appropriate precautions should be taken [8–13]. When Q235-steel is exposed to hydrochloric acid, it can generally react in an electrochemical process, often involving a chemical reaction between the metal (metallic dissolution) and the H^+ ions produced by the dissociation of the acid (release of molecular hydrogen) [2, 4, 9–11]. This reaction can lead to the formation of compounds such as metal salts or oxides, altering the structure of the steel and causing corrosion. This corrosion can have disastrous consequences

on the integrity of equipment and structures, leading to premature failures and significant costs associated with repairs, replacements and production downtime [8, 13].

Proactive management strategies, aimed at mitigating the effects of corrosion in such environments, are essential to maintain operational safety, extend equipment life and reduce maintenance costs in various industrial sectors such as the petrochemical and chemical industries, and other areas where exposure to acids is commonplace. As a result, preventive measures are recommended, including the use of protective coatings, the selection of more corrosion-resistant materials and the use of corrosion inhibitors, *etc.* [8–10].

The development of an effective inhibitor remains a major challenge due to the diversity of organic compounds. Many inhibitors used in acidic environments are organic compounds containing heteroatoms such as nitrogen, sulfur and oxygen [3, 5–7, 14]. Literature data show that most of these compounds act by adsorption onto the metal surface, and that this mode of action depends, among other things, on the nature and charge of the metal surface, the type of aggressive electrolyte and also the chemical structure of the inhibitors.

Promising results obtained with 2-mercaptobenzimidazole and its dimer; 2-(1*H*-benzimidazol-2-yl)disulfanyl)-1*H*-benzimidazole, *S*-alkylated mercaptobenzimidazole derivatives; 1*H*-benzimidazol-2-thiyl hexane and 1*H*-benzimidazol-2-thiyl dodecane for inhibiting corrosion of mild steel in an acidic environment [15–18], acting by adsorption onto the metal surface. These have aroused our interest in extending the application of these compounds to bis-mercaptobenzimidazoles with a carbon chain of variable length. These are the mercapto-benzimidazole bolaform surfactants, designated MB-C_{*n*}-MB with (*n* = 2, 4, 6, 8 & 10). The study consisted in their use, as inhibitors, against the corrosion of Q235-steel exposed to the aggressive 1 M HCl solution. The comprehensive study focused on MB-C₂-MB and MB-C₈-MB, with hydrophobic balance testing for the rest of inhibitors restricted to the optimum concentration of 10^{−3} mol·L^{−1}.

To this end, we carried out weight or gravimetric measurements (mass loss) and stationary electrochemical measurements using potentiodynamic polarization. The *i*–*E* curves are evaluated by three methods (Tafel-Fit, Stern-Fit and *R*_p-Fit) to determine various electrochemical parameters. The main focus is on the polarization curve plotting method and its advantages. This is followed by a qualitative analysis of the curves to highlight certain recurrent and now erroneous interpretations often reported in the literature. Finally, a quantitative analysis based on the use of three theoretical models, all derived from the Wagner–Traud bi-exponential equation, to estimate conventional corrosion process parameters and thus deduce inhibiting efficiencies. Particular attention was paid to the limitations of Tafel's method, based on the exploitation of data at high overvoltage.

In addition, transient electrochemical measurements based on electrochemical impedance spectroscopy were carried out to understand the mechanism of the process taking place at the metal/solution interface, attempting to differentiate each of the elementary steps involved in this process by the difference in their relaxation times. The impedance data obtained, both in the absence and presence of different concentrations of the studied inhibitors, were represented in Cartesian coordinates in the Nyquist complex plane, and in

the Bode and Betova planes translating the frequency behavior of the electrochemical system. These three different views of the same data are not in competition, but rather complementary; each shows a particular aspect of the impedance diagram. The Nyquist representation makes it possible to visualize and even identify the various “loops and/or straights” in the diagram, and possibly masks high-frequency processes, while the Bode and Betova representations offer a complete view of the frequency domain, while being less explicit in identifying certain characteristic processes.

Based on the diverse electrochemical impedance data, several equivalent electrical circuits were constructed and tested to model the electrochemical interface where the processes took place. In addition, the experimental diagrams were superimposed on the theoretical diagrams (from the calculation) to extract the most appropriate set of parameters for a better understanding of the system under study.

Finally, and in order to broaden the scope of this study, six linearized forms of adsorption isotherms corresponding to the Langmuir, Flory–Huggins, Temkin, Frumkin, Freundlich and El-Awady models were developed to simulate adsorption data for the MB-C₈-MB compound. The various parameters inherent in each isotherm were calculated and discussed in order to highlight the adsorption mechanism of this inhibitor at the electrochemical interface. The Langmuir model was critically assessed for its hypothetical nature.

2. Materials and Technique

2.1. Material

The material used in this study is a Q235-steel, it is also known as Q235A according to Chinese standard GB/T 700, whose chemical composition (in mass%) determined by the Castaing microprobe is as follows: C 0.176%, Si 0.233%, Mn 0.570%, S 0.023%, Cu 0.033%, P 0.019%, and the remainder iron (Fe 98.95%) [1–3]. The material was cut into plates of size 4×1×1 cm and coated with a resin so that only 1 cm² of its surface is exposed to the electroactive species present in the aggressive solution. To obtain reliable and reproducible results, the working electrode undergoes before each test, a polishing of the surface with abrasive paper of increasingly fine granulometry: 120-220-400-600-800-1200-2000. In addition, before being dipped in the corrosive solution, the electrode is rinsed with bidistilled water, degreased in acetone, then washed again with bidistilled water and finally dried with forced air before being used.

2.2. Preparation of the corrosive solution

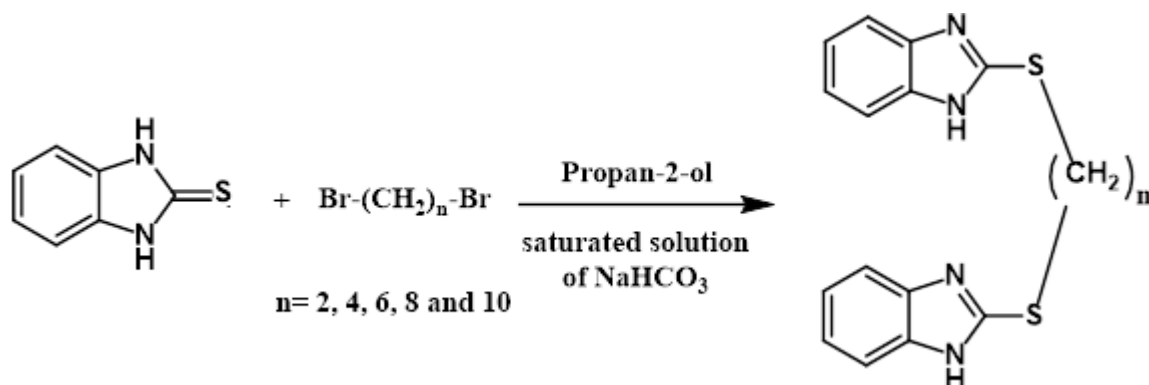
The corrosive solution is a molar hydrochloric acid solution (1 M HCl), obtained by diluting, with bidistilled water, the commercial acid concentrated at 37%. Due to the low solubility in hydrochloric acid of MB-C_n-MB compounds with ($n = 2; 4; 6; 8; 10$), the inhibitors were previously dissolved in dimethylformamide (DMF) at different percentages before the addition of 90 mL of 1 M HCl. The concentration range investigated for the different

inhibitors ranged from 10^{-6} to 10^{-3} mol·L⁻¹. It should be noted that only the optimal concentration of MB-C_n-MB with $n = 4; 6; 10$ was considered due to the similarity of the results and the extensive review was done for MB-C_n-MB compounds with $n = 2$ and 8.

2.3. Inhibitors under study

The studied inhibitors are bolaform surfactants of bis mercapto-benzimidazole type, named 1,2-bis((1*H*-benzo[*d*]imidazol-2-yl)thio)ethane (MB-C₂-MB); 1,4-bis((1*H*-benzo[*d*]imidazol-2-yl)thio)butane (MB-C₄-MB); 1,6-bis((1*H*-benzo[*d*]imidazol-2-yl)thio)hexane (MB-C₆-MB); 1,8-bis((1*H*-benzo[*d*]imidazol-2-yl)thio)octane (MB-C₈-MB); 1,10-bis((1*H*-benzo[*d*]imidazol-2-yl)thio)decane (MB-C₁₀-MB).

The bis-mercaptobenzimidazoles (MB-C_n-MB) mentioned above were resynthesized according to the experimental protocol described in references [19, 20] in satisfactory yields by reacting 1,*n*-dibromoalkanes (Br-C_n-Br) where { $n = 2, 4, 6, 8$ & 10} with benzimidazole-2-thione in propan-2-ol in the presence of a saturated solution of sodium bicarbonate NaHCO₃ (see Scheme 1). We then checked the purity of the synthesized compounds using various characterization methods, to ensure that the compounds were pure and to enable a comparative study of their corrosion inhibition behaviour of Q235-steel in 1 M HCl.



Scheme 1: Synthesis procedure of bis-mercapto-benzimidazole derivatives.

This operation involved dissolving 1 gram of benzimidazole-2-thione, *i.e.* $40 \cdot 10^{-4}$ moles, in a mixture of 40 cm³ of propan-2-ol and a saturated solution of sodium bicarbonate NaHCO₃ (in stoichiometric proportions of {1/1}). To this solution, $35 \cdot 10^{-4}$ moles of 1,*n*-dibromoalkane were added. The resulting reaction mixture was then refluxed for 1 hour and 30 minutes. Once cooled, the precipitated product was filtered, washed with water and recrystallized in ethanol.

All the structures of the MB-C_n-MB compounds obtained were characterized based on spectral data: proton nuclear magnetic resonance (¹H NMR) and mass spectrometry (MS) as follows:

**1,2-bis((1*H*-benzo[*d*]imidazol-2-yl)thio)ethane – {MB-C₂-MB}: C₁₆H₁₄N₄S₂.

This compound was obtained as fine needles in 25% yield, **mp: 256–258°C; **¹H NMR (300 MHz, DMSO-*d*₆) (δ, ppm): 3.75 (s, 4H, CH₂-S), 7.00–7.70 (s, 8H, ArH); *(MS): M⁺ (*m/z*): 326.

**1,4-bis((1*H*-Benzo[*d*]imidazol-2-yl)thio)butane – {MB-C₄-MB}: C₁₈H₁₈N₄S₂.

This compound was obtained as fine needles with 74% yield, **mp: 219–221°C; **¹H NMR (300 MHz, DMSO-*d*₆) (δ, ppm): 7.50–7.80 (m, 8H, ArH); 3.50 (t, 4H, 2 CH₂-S); 2.15 (m, 4H, 2-CH₃); *(MS) M⁺ (*m/z*): 354. **Anal. Calc. for C₂₂H₂₆N₄S₂: C – 61.02; H – 5.08; N – 15.81. **Found: C – 61.17; H – 5.12; N – 15.81.

**1,6-bis((1*H*-Benzo[*d*]imidazol-2-yl)thio)hexane – {MB-C₆-MB}: C₂₀H₂₂N₄S₂.

This compound was obtained as fine needles in 90% yield, **mp: 230–232°C; **¹H NMR (300 MHz, DMSO-*d*₆) (δ, ppm): 7.10–7.36 (m, 8H, ArH); 3.31 (t, 4H, 2 CH₂-S); 1.47 (m, 4H, CH₂); 1.73 (m, 4H, CH₂). *(MS) M⁺ (*m/z*): 382.

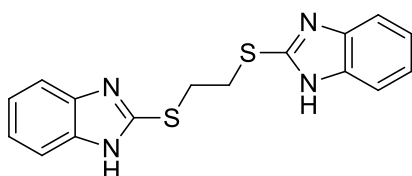
**1,8-bis((1*H*-Benzo[*d*]imidazol-2-yl)thio)octane – {MB-C₈-MB}: C₂₂H₂₆N₄S₂.

This compound was obtained as fine needles in 95% yield, **mp: 233–235°C; **¹H NMR (300 MHz, DMSO-*d*₆) (δ, ppm): 7.10–7.96 (m, 8H, ArH); 3.20 (t, 4H, 2 CH₂-S); 1.55 (m, 12H, 6 CH₂); *(MS) M⁺ (*m/z*): 410. **Anal. Calc. for C₂₂H₂₆N₄S₂: C – 64.8; H – 6.34; N – 13.65. **Found: C – 64.65; H – 6.31; N – 13.57.

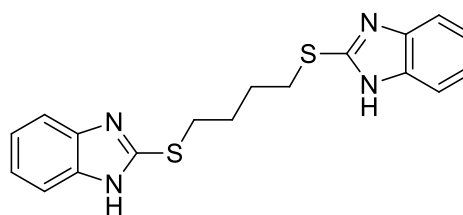
**1,10-bis((1*H*-Benzo[*d*]imidazol-2-yl)thio)decane – {MB-C₁₀-MB}: C₂₄H₃₀N₄S₂.

This compound was obtained as fine needles in 97% yield, **mp: 200–202°C; **¹H NMR (300 MHz, DMSO-*d*₆) (δ, ppm): 7.10–7.50 (m, 8H, ArH); 3.30 (t, 4H, CH₂-S); 1.40 (m, 16H, CH₂) *(MS) M⁺ (*m/z*): 438.

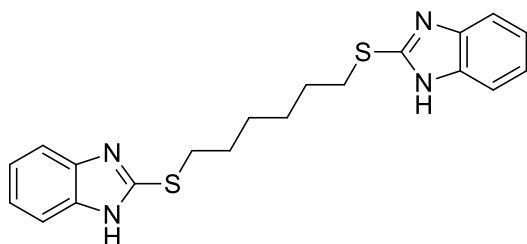
Figure 1 shows the molecular structure of the different inhibitors under study:



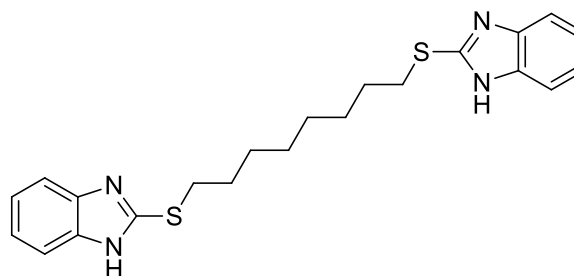
1,2-bis((1*H*-Benzo[*d*]imidazol-2-yl)thio)ethane
(MB-C₂-MB)



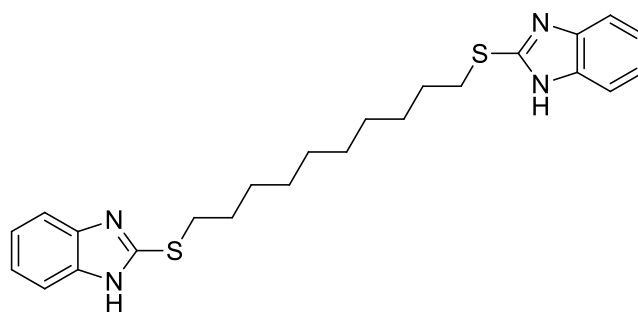
1,4-bis((1*H*-Benzo[*d*]imidazol-2-yl)thio)butane
(MB-C₄-MB)



1,6-bis((1*H*-Benzo[*d*]imidazol-2-yl)thio)hexane (MB-C₆-MB)



1,8-bis((1*H*-Benzo[*d*]imidazol-2-yl)thio)octane
(MB-C₈-MB)

1,10-bis((1H-Benzo[d]imidazol-2-yl)thio)decane (MB-C₁₀-MB)**Figure 1.** Molecular structures of the studied bis mercapto-benzimidazole derivatives.

2.4. Gravimetric and electrochemical methods

The use of electrochemical methods is essential to approach the phenomenon of corrosion and understand its mechanism. However, the gravimetric method, which is easy to implement, and which has the advantage of allowing direct measurement, remains a basic and reference method that reflects the corrosion phenomenon as it is in the real state. However, it is essential to complete the gravimetric tests by stationary and transient electrochemical measurements to be reassured of the validity of the results obtained and for further information on the interfacial processes [4, 12].

2.4.1. Gravimetric tests

Gravimetric experiment is based on the direct measurement of the mass loss ($\Delta m = m_i - m_f$), expressed in mg, undergone by a substrate of section S (cm²), supposedly homogeneous, during a time t (h) of immersion in the corrosive solution maintained at constant temperature. This technique assumes that the corrosion is generalized on the whole surface. The corrosion rate W_{corr} is given by Equation 1, as follows [4]:

$$W_{\text{corr}} = \frac{\Delta m}{S \times t} \left(\text{mg cm}^{-2} \text{ h}^{-1} \right) \quad (1)$$

The inhibiting efficiency of an organic compound is determined by Equation 2 as follows:

$$\eta_{\text{ML}} \% = \left(1 - \frac{W_{\text{corr}}^{\text{inh}}}{W_{\text{corr}}^0} \right) \times 100 \quad (2)$$

where W_{corr}^0 and $W_{\text{corr}}^{\text{inh}}$ represent respectively the values of the corrosion rate of Q235-steel, after immersion, in the absence and presence of each inhibitor.

The mild steel samples used, in square form with dimensions of 4×1×1 cm, are immersed vertically for 6 hours in the corrosive solution in absence of agitation maintained at a constant temperature (298 K). At the end of the experiment, the corrosion products are removed, and the samples are weighed again.

2.4.2. Electrochemical measurements

The stationary electrochemical method is based on the plotting of i – E polarization curves. Starting from the mixed corrosion potential, E_{corr} , a constant potential E is imposed, which disturbs the system on the cathodic or anodic side to examine the behavior in the vicinity of the corrosion potential, and the quasi-stationary current i is measured when the measurement is stabilized [21–22].

The electrochemical tests were carried out in a 3-electrode cell linked to a Bio-Logic VSP VMP3 Potentiostat controlled by the analysis software "Ec-Lab version 10.20". The reference electrode (RE) is a 2nd species electrode with Ag/AgCl/3 M KCl. The auxiliary electrode (CE counter electrode) was a large surface platinum electrode. The working electrode (WE) was identical to the one used for gravimetric measurements and was coated with resin to reduce to 1 cm² the surface exposed to the electroactive species. Before the polarization curves were plotted, the working electrode was held at its open circuit or abundant potential for half an hour. It is to be noted that the working electrode must be placed close to the reference electrode to minimize the ohmic drop. In our case, the electrolytic resistance is low which weakens this potential drop. In this study, all electrochemical measurements were performed at the temperature of 298 K and performed at least twice to ensure reproducibility of results.

The study was conducted in potentiodynamic mode by scanning the sample with a scroll of potentials that vary continuously from ($E_{\text{ocp}}+30$ mV) to -900 mV cathodically and anodically from ($E_{\text{ocp}}-30$ mV) to -100 mV vs. Ag/AgCl/3 M KCl with a scan speed of $\{dE/dt=0.5 \text{ mV}\cdot\text{s}^{-1}\}$. This value is sufficiently low, which makes it possible to approach as closely as possible the steady state conditions of the system studied [21, 22]. Indeed, the double sweep adopted in the present work is designed to avoid the impact of high electrode polarization on the data recorded in the vicinity of the corrosion potential. In other words, the curve is plotted from low polarization to high polarization.

The perturbations of Q235-steel/1 M HCl electrochemical system, in the absence and presence of inhibitors, were performed after 30 min of stabilization at the open circuit potential of the electrochemical system. It should be noted that after only 30 min of stabilization, the working electrode takes a constant potential with respect to the solution called corrosion potential.

Non-stationary or transient techniques were based on the perturbation of the physical quantities of the electrochemical system so that the response of the system can be analyzed in a linear time invariant domain. These techniques have been developed to overcome several constraints that arise when a researcher wants to estimate the metal resistance or when he studies the reaction mechanisms involved. Theoretically, this technique allows differentiating the reaction processes by their relaxation times by applying a low amplitude sinusoidal potential perturbation of 10 mV peak to peak around the stationary value of E_{ocp} at the working electrode over a frequency range from 100 kHz {HF} to 100 mHz {LF} with five points per decade to receive such a sinusoidal response in current [23–28]. The electrode

is held at E_{corr} for 30 min at temperature 298 K, before each measurement. It is noted that this technique is not very destructive for the interface because the potential variation imposed around the corrosion potential is low [28].

3. Results and Discussion

First, we examined the effect of MB-C₂-MB and MB-C₈-MB concentration by coupling the mass loss (ML) method with stationary (PP) and transient electrochemical (EIS) methods.

3.1. Mass loss measurements

The gravimetric method is the first approach to directly access to the inhibiting efficiency and corrosion rate at different concentrations of both surfactants MB-C₂-MB and MB-C₈-MB after 30 min of immersion in 1 M HCl at the temperature of 298 K in atmospheric air. For all concentrations, the mean value of the corrosion rate W_{corr} and the inhibition efficiency $\eta_{\text{ML}}\%$ are calculated using Equations 1 and 2. The variations in the corrosion rate of mild steel and the corresponding efficiency at different concentrations of MB-C₂-MB and MB-C₈-MB in 1 M HCl medium are illustrated in Figure 2.

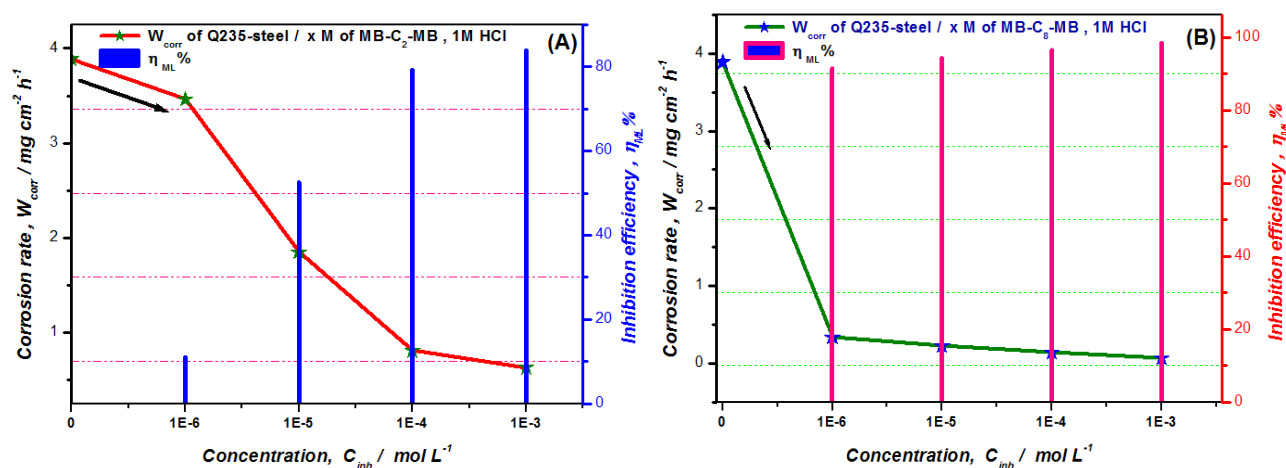


Figure 2. Evolutions of the corrosion rate W_{corr} and the corresponding inhibition efficiency $\eta_{\text{ML}}\%$ versus concentrations of MB-C₂-MB and MB-C₈-MB

Inspection of Figure 2 shows that the corrosion rate of Q235-steel is considerably reduced with the addition of MB-C₈-MB and ostensibly less markedly in the presence of MB-C₂-MB. Indeed, for the aggressive solution alone, the uninhibited medium, the rate drops from $3.89 \text{ mg} \cdot \text{cm}^{-2} \cdot \text{h}^{-1}$, for the reference solution, to $0.0653 \text{ mg} \cdot \text{cm}^{-2} \cdot \text{h}^{-1}$ at 10^{-3} M of MB-C₈-MB and to only $0.6321 \text{ mg} \cdot \text{cm}^{-2} \cdot \text{h}^{-1}$ at the same concentration of MB-C₂-MB. On the other hand, the inhibiting efficiency is significantly improved and reaches a maximum value of 98% and 83% at 10^{-3} M concentration in the presence of MB-C₈-MB and MB-C₂-MB, respectively. This finding can be justified by the formation of a more persistent protective barrier in the presence of MB-C₈-MB than with MB-C₂-MB that hinders the infiltration and thus the electronic exchange between the iron metal and the electroactive

species (H^+ protons) as well as the aggressive anion Cl^- , which can hardly be adsorbed onto Q235-steel surface.

It can be concluded that these two heterocyclic bolaform surfactants possess interesting corrosion-inhibiting properties for Q235-steel in a molar hydrochloric environment, with the MB-C₈-MB compound showing excellence.

3.2. Steady-state electrochemical study: Polarization curves

The gravimetric study remains a direct and basic method, which best reflects the corrosion phenomenon as it is in the real state. However, it has the disadvantage of not approaching the mechanism involved during corrosion [12]. To ensure the validity of the obtained results, it becomes imperative to complete these gravimetric tests by indirect electrochemical measurements: stationary {DC} and transient {AC} [27].

The stationary electrochemical measurements allow collecting information related to the thermodynamics and kinetics of the studied system since they consider only the kinetically determining stage among all the elementary stages of the global corrosion process taking place at the metal/solution interface. Nevertheless, they are subject to limitations, especially in the case of very resistant systems or for the study of reaction mechanisms. Moreover, some of them lead to the sample destruction. To overcome these limitations, a few so-called transient techniques have been developed, based on the use of transfer functions, of which EIS is one (*cf.* hereafter).

Potentiodynamic polarization measurements can be used to collect more information related to the system being investigated. The cathodic and anodic polarization curves of Q235-steel in 1 M HCl medium obtained in the absence and presence of different concentrations of MB-C₂-MB and MB-C₈-MB at 298 K, are shown in Figure 3.

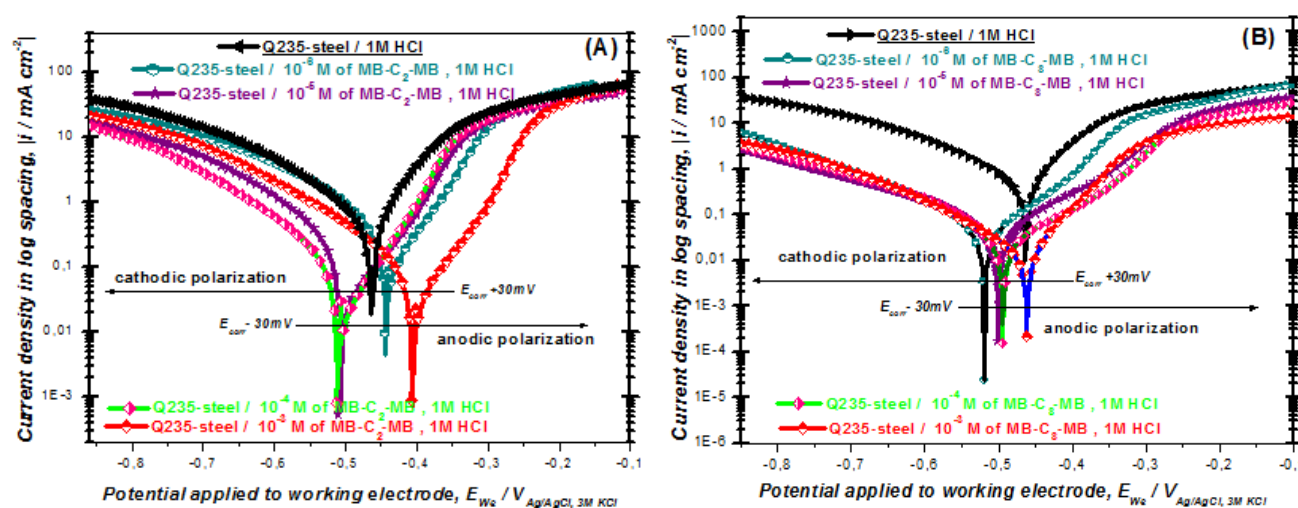


Figure 3. Polarization curves of Q235-steel in 1 M HCl obtained at temperature 298 K without and with addition of inhibitors at concentrations ranging from 10^{-6} to 10^{-3} M: (A) MB-C₂-MB, (B) MB-C₈-MB.

3.2.1. Qualitative analysis by visual inspection of polarization curves

A first reading of polarization curves (A) and (B) reveals that both cathodic and anodic branches are affected to different degrees following the addition of MB-C₂-MB and MB-C₈-MB inhibitors. Indeed, for MB-C₂-MB, at 10⁻³ M, anodic current densities are significantly lower than cathodic ones compared to blank {1 M HCl}, whereas for lower concentrations, current attenuations are comparable. It is highly interesting to note that the cathodic curve, at 10⁻³ M in MB-C₂-MB, is positioned above those corresponding to lower concentrations. This observation will be interpreted later to clarify what is widely reported in the literature, namely that the lower the curve, the lower the resulting current density [12].

Nevertheless, in the presence of MB-C₈-MB, cathodic current densities, presumably unaffected by concentration, are clearly lower compared to blank and relatively lower compared to their anodic counterparts. Furthermore, a slight shift in corrosion potential is recorded at the more cathodic potentials in the presence of MB-C₈-MB except at 10⁻³ M where E_{corr} remains almost constant, while this last, in the presence of different concentrations of MB-C₂-MB, has shifted slightly to both sides of that of the corrosive solution alone and this shift does not follow a particular order as a function of its concentration. These observations confirm the mixed nature of the two inhibitors [4, 23] and clearly show that the addition of these inhibitors, at different concentrations, reduces both the anodic dissolution of steel described by the reaction given by Equation 3 and the discharge of H⁺ protons given by Equation 4:



Based on the aforementioned data, it can be concluded that MB-C₈-MB adsorbs preferentially on cathodic sites when added to the corrosive medium and covers more cathodic than anodic sites on the steel surface as its concentration increased. On the other hand, MB-C₂-MB is poised to play a predominantly anodic inhibiting role at 10⁻³ M, while for the rest of the concentration range; a mixed behavior is more noticeable.

Examination of the cathodic branches of these polarization curves shows that they exhibit excellent linearity (nice straight lines) over a wide potential range (more than a decade in current) from $E_{\text{corr}} - 80$ mV to $E_{\text{corr}} - 200$ mV, indicating that Tafel's law is indeed verified in the cathodic range and that the H⁺ proton discharge reaction is well controlled by pure activation kinetics [4, 12, 23].

Examination of the anodic branches, on the other hand, shows little evidence of Tafel behavior, and the mode of inhibition remains dependent on electrode potential. Indeed, for all inhibitor concentrations studied, we observe the presence of two linear portions in the case of high over potentials. In fact, at potentials above $-0.3 \text{ V}_{\text{Ag/AgCl/3M}}$ (the so-called desorption potential, E_d , or non-polarizability potential), the presence of MB-C₈-MB and MB-C₂-MB has virtually no effect on the anodic curves, and the anodic current density rises rapidly, leading to pronounced dissolution in the region of high overvoltage [21, 23, 27].

The anodic curves return to the blank one, indicating electrode exposure in the case of MB-C₂-MB at all concentrations, and similar behavior at 10⁻⁶ M for MB-C₈-MB, whereas at higher concentrations the cathodic branch remains lower, albeit at high over potentials. This behavior has been extensively documented in the literature, particularly in the case of various studies on the inhibition of steel corrosion in hydrochloric media [12]. The rapid increase in anode current after E_d potential is attributed to the inhibitor molecules desorption due to strong polarization of the working electrode [4, 6, 13, 17, 25–27].

3.2.2. Quantitative analysis of polarization curves using three methods

The extraction of electrochemical parameters from i – E polarization curves was carried out using the three methods Tafel-Fit, Stern-Fit and R_p -Fit, which exploits these i – E curves differently, depending on the range of potentials undertaken. In fact, Tafel's law exploits the linear part of the anodic and cathodic branches located between ± 80 mV and ± 200 mV around E_{corr} using linear regression (high η overvoltage) [4, 12]. As for Stern's or Wagner–Traud law, the potential range explored, using a non-linear regression (bi-exponential relationship), is limited to the vicinity of the corrosion potential; ± 100 mV [29, 30] (medium η overvoltage). Jena and Bonhoeffer method (R_p -Fit), also known as the linear polarization resistance law is limited to the immediate vicinity of E_{corr} to ± 25 mV (relatively low η overvoltage) [12, 22, 25, 31].

3.2.2.1. Parameters extraction using the Tafel method

Tafel fitting results are obtained each time a marker is moved. The default positions of the markers are ± 80 mV to ± 200 mV around E_{corr} , *i.e.*, the potential range explored, to deduce the electrochemical parameters, is located beyond ± 80 mV with respect to E_{corr} and within a potential range of ± 120 mV conditioned by good linearity of the corresponding curves. The software deduces the open-circuit potentials E_{corr} , from the intersection of Tafel's linear regressions and the straight vertical line passing through $E = E_{\text{corr}}$, which corresponds to zero overall current ($i=0$) [27, 32].

In the present study, the values of corrosion current densities, cathodic Tafel slopes and corrosion potentials are determined by extrapolating cathodic Tafel lines to corrosion potentials using the software (Ec-Lab, Bio-Logic). We have confined ourselves exclusively to the cathodic branches, as they meet the conditions for use of the Tafel method, whereas the anodic branches are difficult to use for the reasons described above [21, 27]. Several authors [4, 11–13, 23–25] have adopted this method for the determination of when anode branches are difficult to highlight. Table 1 lists all the electrochemical parameters obtained by Tafel's method. The corrosion inhibiting efficiency values obtained from the Tafel method is calculated according to Equation 5:

$$\eta_{\text{Tafel-Fit}} \% = \left(1 - \frac{i_{\text{corr}}^{\text{inh}}}{i_{\text{corr}}^0}\right) \times 100 \quad (5)$$

where $i_{\text{corr}}^{\text{inh}}$ and i_{corr}^0 represent the corrosion current density values, with and without inhibitors, respectively.

Analysis of the electrochemical parameters given in Table 1 reveals that corrosion current densities decreases considerably in the presence of MB-C₈-MB than in the presence of MB-C₂-MB with increasing concentrations, reaching, at 10^{−3} M, minimum current density values of around 47.55 $\mu\text{A}\cdot\text{cm}^{-2}$ and 148.13 $\mu\text{A}\cdot\text{cm}^{-2}$, respectively. Consequently, the inhibition efficiency increases to reach its maximum value of 83%, at 10^{−3} M, of MB-C₂-MB and 97% at the same concentration of MB-C₈-MB. This behavior suggests that the protective adsorption film formed onto the steel surface tends to be increasingly compact and stable with increasing inhibitor concentration along with surfactant hydrophobic chain length.

Table 1. Sets of electrochemical parameters evaluated by the Tafel method from the cathodic branches of the i – E curves for Q235-steel in 1 M HCl without and with addition of different concentrations of MB-C₂-MB and MB-C₈-MB at 298 K.

Method	Tafel–fit				
Interface	E_{corr} , mV _{Ag/AgCl} , 3M KCl	I_{corr} , $\mu\text{A}\cdot\text{cm}^{-2}$	$-\beta_{\text{c}}\%$, mV $\cdot\text{dec}^{-1}$	$\eta_{\{\text{Tafel-fit}\}}\%$	Θ_{Tafel}
Q235-steel/1 M HCl	−463.58	789.48	179.5	–	
Q235-steel/10 ^{−6} M of MB-C ₂ -MB, 1 M HCl	−443.20	645.41	198.7	18.24	0.18
Q235-steel/10 ^{−5} M of MB-C ₂ -MB, 1 M HCl	−506.50	389.44	173.5	50.67	0.50
Q235-steel/10 ^{−4} M of MB-C ₂ -MB, 1 M HCl	−512.40	194.27	157.7	75.29	0.75
Q235-steel/10 ^{−3} M of MB-C ₂ -MB, 1 M HCl	−407.03	148.13	163.3	81.23	0.81
Q235-steel/10 ^{−6} M of MB-C ₈ -MB, 1 M HCl	−519.47	101.98	163.4	87.08	0.87
Q235-steel/10 ^{−5} M of MB-C ₈ -MB, 1 M HCl	−500.42	99.30	204.2	87.42	0.87
Q235-steel/10 ^{−4} M of MB-C ₈ -MB, 1 M HCl	−494.15	85.73	174.3	89.14	0.89
Q235-steel/10 ^{−3} M of MB-C ₈ -MB, 1 M HCl	−461.59	47.55	142.2	93.97	0.93

The mixed nature of the behavior of the two surfactants described above is confirmed by the slight shift in corrosion potential, which varies cathodically and anodically in the range of 43–49 mV and 2–56 mV, in the presence of MB-C₂-MB and MB-C₈-MB,

respectively compared to the uninhibited solution. According to the literature, it has been found that if the shift is greater than 80 mV, the inhibitor can be considered either a cathodic or anodic type inhibitor, whereas when the shift is less than 80 mV, the inhibitor can be classified as mixed type [8, 33, 34]. Consequently, the results obtained above shows that the shift in potentials hardly exceeds 80 mV at different concentrations of MB-C₂-MB and MB-C₈-MB, confirming their mixed character, *i.e.*, that they adsorb both anodic and cathodic sites onto the steel surface. Furthermore, the values of the cathodic Tafel slopes obtained in the presence of the two inhibitors at different concentrations vary by around $\pm 30 \text{ mV} \cdot \text{dec}^{-1}$ from that of the blank, implying that their influence on the cathodic reaction only slightly modifies the proton discharge mechanism [4]. This result suggests that the quantitative analysis of the curves runs counter to the qualitative one. Indeed, at 10^{-3} M , the curve for the MB-C₂-MB inhibitor is placed above those for the rest of the concentrations, and so it was expected that the corresponding current density would now be higher. In practice, however, this is not the case, and we must therefore be wary of jumping to hasty conclusions based on the simple visual inspection often encountered in the literature. The assessment of current density depends on both the Tafel slope and the corrosion potential. This being the case, the location of the branches is no guarantee of simple development of ideas on corrosion current. Hence, comparing the arrangement of the polarization curve branches at each inhibitor concentration in the high overvoltage range to compare the inhibiting efficiency and effect on the anodic and cathodic reactions is only valid when their corrosion potentials are close. Comparing polarization curve branches with different corrosion potentials distorts interpretations of corrosion current densities and corresponding inhibiting efficiencies. For example, at 10^{-3} M of MB-C₂-MB, the inhibiting efficiency is higher than at 10^{-5} M , even though the cathodic branch corresponding to the 10^{-3} M concentration is located above the branch corresponding to 10^{-5} M . Similar findings are observed at 10^{-4} M .

On the other hand, Mansfeld and Lorenz [21, 27] point out that Tafel extrapolation, also known as the intercept method, has the disadvantage of requiring data recorded at high overvoltage. In these regions, the net current flow is intense, so strong polarization can lead to changes in surface structure, particularly anodic polarization [23, 25]. The result is a change in surface activity and the influence of secondary reactions taking place at the interface [21, 22]. To overcome these complications associated with Tafel's assumptions, we resorted to parameter estimation using the Stern and Jena and Bonhoeffer methods.

3.2.2.2. Parameters extraction using the Stern method

It is also very interesting to find corrosion kinetic parameters from a non-linear fit, as stated above, of the experimental data to Stern's Equation 6 using graphical data analysis software (Origin pro, Origin-Lab).

$$i = i_a + i_c = i_{\text{corr}} \times \left[\exp(b_a \times (E - E_{\text{corr}})) - \exp(b_c \times (E - E_{\text{corr}})) \right] \quad (6)$$

where b_a and b_c are the Tafel constants (V^{-1}) of the anodic and cathodic reactions, respectively. These constants are related to the Tafel slopes β ($V \cdot \text{dec}^{-1}$), in the natural logarithmic scale, by the following Equation 7:

$$\beta = \frac{\ln 10}{b} \quad (7)$$

For the potential range which is not too far from the corrosion potential and extends up to $E_{\text{corr}} \pm 100$ mV, the overall values of the current densities i , are considered to be the sum of the contributions of the anodic and cathodic current densities i_a and i_c . However, in the present work, the potential range explored, in the absence and the presence of the different concentrations of MB-C₂-MB and MB-C₈-MB, is between $E_{\text{corr}} - 100$ mV and $E_{\text{corr}} + 30$ mV. Figure 4 shows the results of non-linear fitting of the different polarization curves obtained in the absence and presence of different concentrations of MB-C₂-MB and MB-C₈-MB by Stern's method.

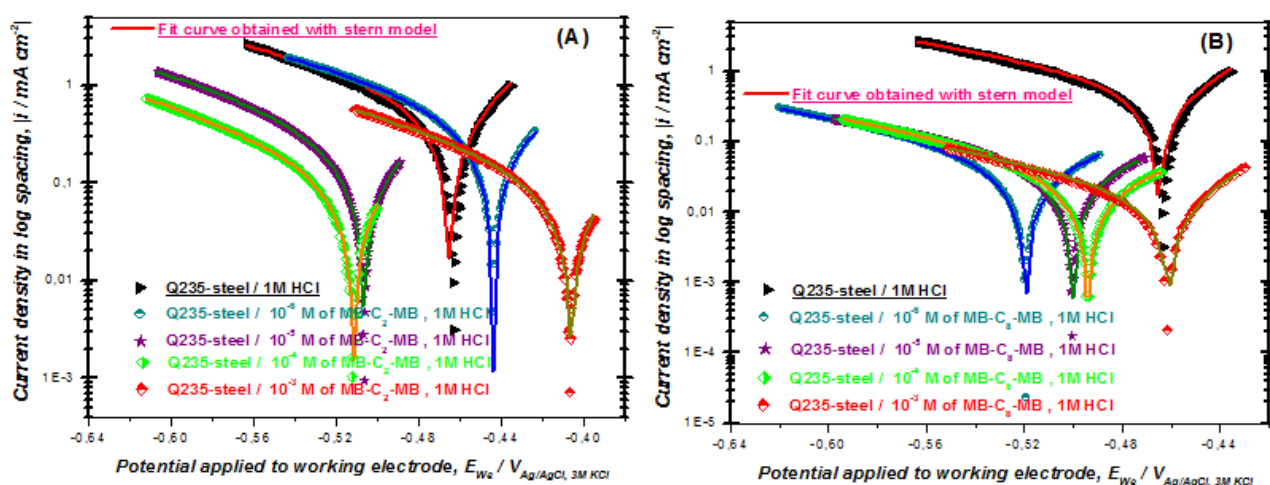


Figure 4. Experimental and simulated i – E curves using the Stern model of Q235-steel in 1 M HCl medium, in the absence and presence of different concentrations of MB-C₂-MB and MB-C₈-MB.

An initial analysis shows that the good superposition observed between the various experimental polarization curves and the corresponding simulated ones, attests to the excellent parametric fit of the experimental data using the Stern's model. Figure 4 clearly shows that the addition of MB-C₂-MB and MB-C₈-MB to 1 M HCl corrosive solution reduces both the anodic dissolution of iron and the cathodic hydrogen evolution reaction.

The inhibition efficiencies $\eta_{\text{Stern}}^{i_{\text{corr}}}$ and $\eta_{\text{Stern}}^{R_p^{\text{calc}}}$ evaluated by equation 8 and 11, as well as those of the electrochemical parameters (E_{corr} , i_{corr} , β_a , β_c , R_p^{calc}) derived from parametric fitting of the experimental data of the different polarization curves in Figure 4 using a nonlinear regression with Stern's equation (6), the coefficient of determination R^2 , and the error factor χ^2 are presented in Table 2.

Table 2. Electrochemical parameter sets evaluated by non-linear regression of i – E curves at [$E_{\text{corr}} - 100$ mV; $E_{\text{corr}} + 30$ mV] using Stern's method and corrosion inhibition efficiencies of Q235-steel in 1 M HCl without and with addition of different concentrations of MB-C₂-MB and MB-C₈-MB at 298 K.

Method	Stern–fit					Statistical parameters		Calculated parameters			
Interface	E_{corr} , mV Ag/AgCl, 3 M KCl	i_{corr} , $\mu\text{A} \cdot \text{cm}^{-2}$	b_a , V^{-1}	b_c , V^{-1}	$\eta_{\{\text{Stern}\text{-fit}\}}\%$	χ^2	R^2	β_a , $\text{mV} \cdot \text{dec}^{-1}$	$-\beta_c$, $\text{mV} \cdot \text{dec}^{-1}$	R_p , cal	$\eta_{\{\text{S-G}\}}$
Q235-steel/1 M HCl	-465.06 ± 0.160	685.05 ± 6.64	–	–	–	0.00305	0.9992	86.26	168.23	36.15	–
Q235-steel/ 10^{-6} M of MB-C ₂ -MB, 1 M HCl	-443.640 ± 0.001	593.79 ± 0.02	–	–	13.32	0.00001	1	97.44	184.85	46.66	22.52
Q235-steel/ 10^{-5} M of MB-C ₂ -MB, 1 M HCl	-506.520 ± 0.002	337.32 ± 0.02	–	–	50.76	0.00001	1	109.65	156.63	83.03	56.46
Q235-steel/ 10^{-4} M of MB-C ₂ -MB, 1 M HCl	-511.690 ± 0.040	146.62 ± 1.12	–	–	78.59	0.00260	0.9999	127.89	140.20	198.10	81.75
Q235-steel/ 10^{-3} M of MB-C ₂ -MB, 1 M HCl	-406.160 ± 0.050	111.19 ± 0.74	–	–	83.77	0.00194	0.9999	107.90	146.50	242.69	85.10
Q235-steel/ 10^{-6} M of MB-C ₈ -MB, 1 M HCl	-519.50 ± 0.001	66.58 ± 0.55	–	–	90.28	0.00400	0.9992	147.94	149.62	485.34	92.55
Q235-steel/ 10^{-5} M of MB-C ₈ -MB, 1 M HCl	-500.51 ± 0.001	66.46 ± 0.29	–	–	90.29	0.00100	0.9997	148.59	183.91	537.20	93.27
Q235-steel/ 10^{-4} M of MB-C ₈ -MB, 1 M HCl	-493.94 ± 0.001	53.82 ± 0.09	–	–	92.14	0.00500	0.9978	237.16	160.56	772.77	95.32
Q235-steel/ 10^{-3} M of MB-C ₈ -MB, 1 M HCl	-461.20 ± 0.001	17.01 ± 0.05	–	–	97.51	0.00100	0.9949	064.52	131.32	1104.63	96.72

The inhibition efficiency derived from Stern's method $\eta_{\text{Stern}}\%$ is calculated using the corrosion current densities obtained in the presence $i_{\text{corr/inh}}$ and absence i_{corr} of inhibitor according to Equation 8, which is identical in terms of expression to Equation 5:

$$\eta_{\text{Stern}}^{i_{\text{corr}}}\% = \left(1 - \frac{i_{\text{corr/inh}}}{i_{\text{corr}}}\right) \times 100 \quad (8)$$

Furthermore, using the polarization resistances calculated R_p^{calc} according to equation (9) from the values of i_{corr} , β_a , β_c obtained in the absence and presence of different inhibitor concentrations, we can trace the corresponding inhibitory efficiencies $\eta_{\text{Stern}}^{R_p^{\text{calc}}}$ according to Eq. 11:

$$R_p^{\text{calc}} = \frac{C}{i_{\text{corr}}} \quad (9)$$

$$C = \frac{\beta_a \times \beta_c}{2.303 \times (\beta_a + \beta_c)} \quad (10)$$

$$\eta_{\text{Stern}}^{R_p^{\text{calc}}}\% = \left(1 - \frac{R_p^{\text{calc}}}{R_{p/\text{inh}}^{\text{calc}}}\right) \times 100 \quad (11)$$

where $R_{p/\text{inh}}^{\text{calc}}$ and R_p^{calc} are the polarization resistance values of steel with and without inhibitor, respectively calculated according to Equation 9 [12, 25]. The accuracy of the regression can be estimated with χ^2 according to Equation 12:

$$\chi^2 = \frac{1}{N} \sqrt{\sum_{i=1}^N \frac{(i_{\text{mes},i} - i_{\text{cal},i})^2}{D_i^2}} \quad (12)$$

where N is the degree of freedom, $i_{\text{mes},i}$ denotes the measured data, while $i_{\text{cal},i}$ corresponds to the model data, calculated from the Stern equation.

A very good correlation between experimental and simulated data is observed by the good superposition of experimental and fitted curves illustrated in Figure 4, as evidenced by the value of the very low χ^2 error factor in the presence of MB-C₂-MB and MB-C₈-MB at different concentrations. This factor represents the mean square deviation between the Stern model and experimental values, and thus assesses the accuracy of the modeling. High values of the coefficient of determination R^2 , measuring the closeness of the experimental data to the fitted regression line, indicate that the experimental data are well described by the Stern model.

Furthermore, examination of the Stern model fitting results of Table 2, once again attests to the trend observed with the Tafel method results in terms of corrosion currents and thus inhibitor efficiencies as a function of inhibitor concentration. However, it should be noted that, for the same concentration, the corrosion current density derived from Stern's method is revised downwards compared with that derived from Tafel's method. This result can be attributed to the difference in cathodic slopes between the two methods. Such a

change is likely to be due to the impact of the strength of polarization, especially as it moves away from E_{corr} , which generates a different activity of the surface state (secondary reactions, concentration polarization...) and consequently different current densities.

Furthermore, the calculated values of polarization resistance (Equation 9) increase with the concentration of both inhibitors, rising from $36.15 \Omega \cdot \text{cm}^2$ for the corrosive solution alone to a value of $242.69 \Omega \cdot \text{cm}^2$ at 10^{-3} M in MB-C₂-MB and to $1.104 \text{ k}\Omega \cdot \text{cm}^2$ at the same concentration in MB-C₈-MB. Thus, the calculated inhibitory efficiencies $\eta_{\text{Stern}}^{\text{icorr}}$ and $\eta_{\text{Stern}}^{\text{R}_{\text{p}}^{\text{calc}}}$ follow the same trend with a maximum value of 85% and 97% respectively at 10^{-3} M concentration in MB-C₂-MB and MB-C₈-MB.

3.2.2.3. Parameters extraction using the Jena–Bonhoeffer method (R_p -Fit)

As the polarization resistance is inversely proportional to the corrosion current, the inhibiting efficiency $\eta_{R_p\text{-Fit}}\%$ is determined by Equation 13:

$$\eta_{R_p\text{-Fit}}\% = \left(1 - \frac{R_p}{R_{p/\text{inh}}}\right) \times 100 \quad (13)$$

R_p and $R_{p/\text{inh}}$ are the polarization resistances of the steel without and with the addition of the inhibitor, respectively.

Figure 5 illustrates the method for determining polarization resistance using the Jena and Bonhoeffer method, based on linear regression of $E=f(i)$ polarization curve data in the vicinity of E_{corr} , corresponding to 1 M HCl corrosive solution alone.

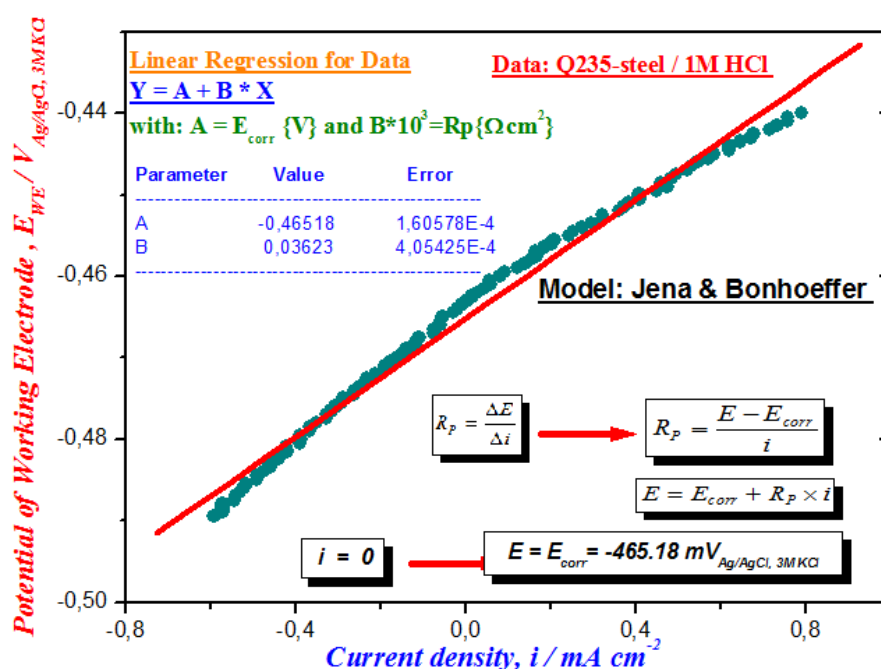


Figure 5. Linear regression of the polarization curve ($E-i$) of Q235-steel obtained at 298 K in 1 M HCl.

The polarization resistance of Q235-steel, obtained following the example of the linear polarization domain in 1 M HCl in the absence and presence of MB-C₂-MB and MB-C₈-MB at different concentrations, and the resulting inhibiting efficiencies estimated by Equation 13, are also reported in Table 3.

Analysis of these results shows that the polarization resistance of the steel, and the resulting inhibiting efficiency, increases with increasing concentration of MB-C₂-MB and MB-C₈-MB inhibitors, reaching a value of 85% for MB-C₂-MB and 97% for MB-C₈-MB at the same concentration of 10^{−3} M. This behavior is probably due to the displacement of water molecules (solvent molecules) by the adsorption of the inhibitor's organic molecules onto the metal surface, resulting in the formation of a stable, persistent film that reduces the corrosion rate by blocking the anodic and/or cathodic sites associated respectively with metal dissolution and proton reduction reactions in solution [23–25].

Table 3. Electrochemical parameter sets obtained from polarization curves of mild Q235-steel in 1 M HCl at different inhibitor concentrations using the Jena–Bonhoeffer method.

Method	Jena–Bonhoeffer method or R_p -Fit				
Interface	$E_{\text{corr}},$ mV _{Ag/AgCl, 3 M KCl}	$R_p \{R_p\text{-fit}\}$	$\eta\{R_p\text{-fit}\}$	R^2	$\Theta \{R_p\text{-fit}\}$
Q235-steel/1 M HCl	−465.270±0.007	36.001±0.001	–	0.99350	
Q235-steel/10 ^{−6} M of MB-C ₂ -MB, 1 M HCl	−443.652±0.017	42.320±0.072	14.93	0.99992	0.15
Q235-steel/10 ^{−5} M of MB-C ₂ -MB, 1 M HCl	−506.622±0.022	78.686±0.162	54.24	0.99984	0.54
Q235-steel/10 ^{−4} M of MB-C ₂ -MB, 1 M HCl	−511.805±0.045	199.050±0.798	81.91	0.99946	0.82
Q235-steel/10 ^{−3} M of MB-C ₂ -MB, 1 M HCl	−406.488±0.049	246.707±1.097	85.41	0.99935	0.82
Q235-steel/10 ^{−6} M of MB-C ₈ -MB, 1 M HCl	−519.038±0.002	485.000±0.015	92.57	0.99980	0.92
Q235-steel/10 ^{−5} M of MB-C ₈ -MB, 1 M HCl	−500.811±0.012	533.000±0.137	93.24	0.99970	0.93
Q235-steel/10 ^{−4} M of MB-C ₈ -MB, 1 M HCl	−493.162±0.035	780.000±0.978	95.38	0.99870	0.95
Q235-steel/10 ^{−3} M of MB-C ₈ -MB, 1 M HCl	−464.135±0.009	1069.000±1.321	96.66	0.98970	0.97

The polarization resistance estimated by the Jena–Bonhoeffer method is very similar to that calculated using the Stern–Geary formula and the parameters β_a , β_c and i_{corr} derived from the Stern method. The various results obtained using this stationary technique show

that inhibiting efficiencies estimated at high overvoltage (Tafel lines), at medium overvoltage ± 80 mV around E_{corr} (Stern non-linear regression), as well as at low overvoltage (polarization resistance) follow the same trend at each concentration.

However, this stationary electrochemical technique remains inadequate for characterizing complex mechanisms involving several reaction stages with different characteristic kinetics (as is the case with corrosion inhibition processes). The use of transient techniques is therefore essential.

3.3. Transient electrochemical study: EIS Measurements

3.3.1. Graphical analysis of electrochemical impedance diagrams

For a clear understanding of the process mechanism taking place at the electrode/solution interface, electrochemical impedance spectroscopy (EIS) is a very useful technique in investigating corrosion inhibition processes [4]. The Nyquist, Bode and Betova ($-Im(Z)$ vs. f in log spacing) and ($|Im(Z)|$ in log spacing vs. f in log spacing) diagrams of Q235-steel immersed in the corrosive solution 1 M HCl, without and with the addition of MB-C₂-MB and MB-C₈-MB at different concentrations, in these two planes, is illustrated in Figures 6 and 7.

The Nyquist diagrams show one single capacitive loop with a center located below the axis of the real part of the impedance. This indicates, referring to literature [6, 8–13], that corrosion of Q235-steel is essentially controlled by the charge transfer process, which takes place simultaneously with the double layer capacitive process. Such a result indicates that the measured capacitive response is not ideal. This deviation of the Nyquist diagrams with respect to a perfect semicircle is generally explained by the representations of Cole-Cole [35, 36], and/or Cole-Davidson [37] inherent to frequency dispersion or capacity change as a function of frequency. This phenomenon is usually attributed to various physical processes such as inhomogeneity of the electrode surface or its roughness during the corrosion process [4, 8–10], adsorption of inhibitors [38] or formation of porous layers [39, 40]. Note that the size of the loop increases with the concentration of the inhibitor. This suggests that nothing prevents the possibility of a second time constant, albeit indistinguishable from the first.

To confirm or refute this charge transfer mechanism, it was very useful to examine the Betova planes and Bode diagrams, which explicitly reveal the high-frequency information [4]. Indeed, the Bode diagrams and ($-Im(Z)$ vs. $\log f$) show that a single time constant is discernible, justified by the appearance of a single maximum at the phase and imaginary part for all MB-C₂-MB and MB-C₈-MB concentrations.

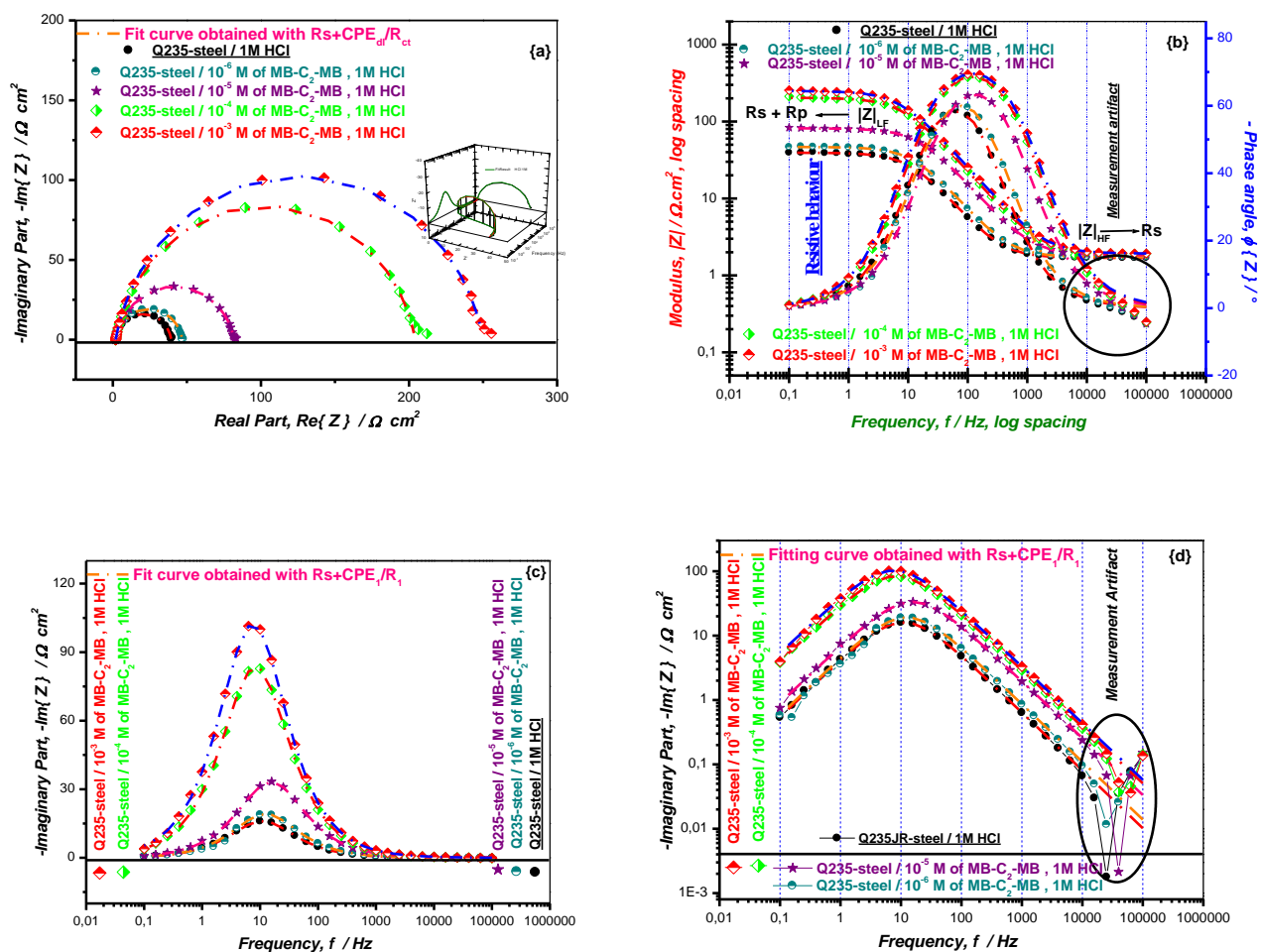
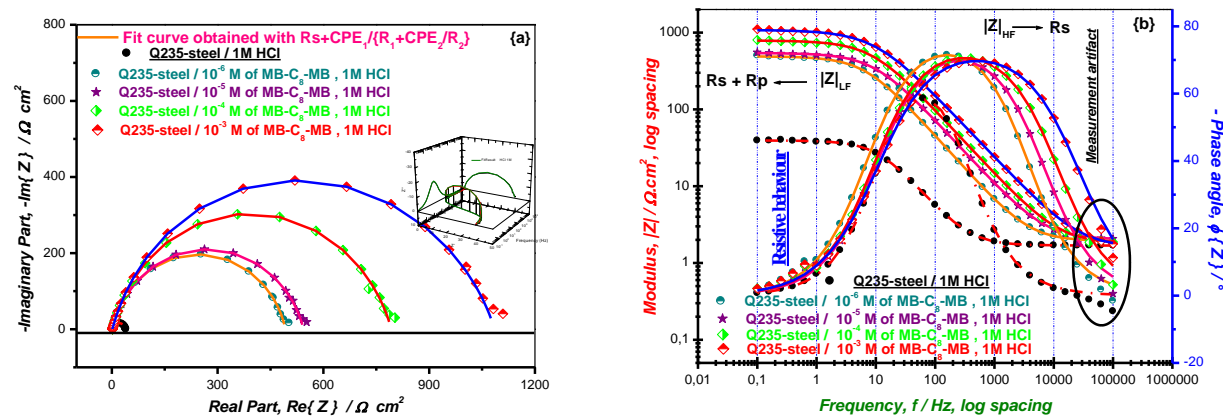


Figure 6. Nyquist {a}, Bode {b}, ($-Im(Z)$ vs. f in log spacing) {c} and ($|Im(Z)|$ in log spacing vs. f in log spacing) {d} diagrams for mild Q235-steel in 1 M HCl at different concentrations of MB-C₂-MB recorded at open circuit potential and at 298 K after 30 min of immersion.



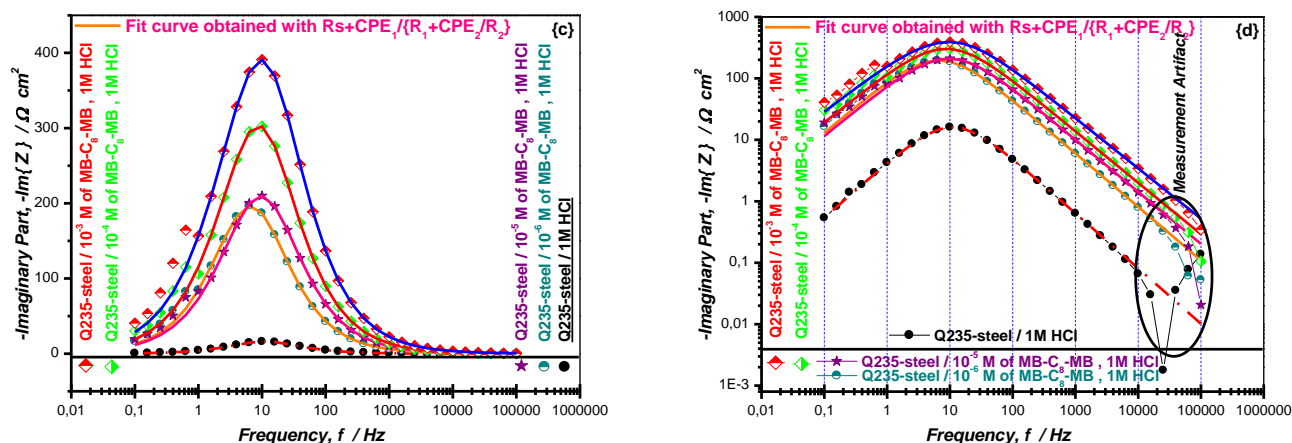


Figure 7. Nyquist {a}, Bode {b}, $(-Im(Z) \text{ vs. } f \text{ in log spacing})$ {c} and $(|Im(Z)| \text{ in log spacing vs. } f \text{ in log spacing})$ {d} diagrams for mild Q235-steel in 1 M HCl at different concentrations of MB-C₈-MB recorded at open circuit potential and at 298 K after 30 min of immersion.

However, we observe that the width at half maximum of the Gaussian ($\phi(Z) \text{ vs. } \log f$) as well as $(-Im(Z) \text{ vs. } \log f)$ obtained in the presence of the different concentrations of MB-C₈-MB is much larger than that obtained in the presence of different concentrations of MB-C₂-MB and 1 M HCl alone. This result likely suggests the appearance of a second time constant, although not well separated from that of the charge transfer in the presence of the different MB-C₈-MB concentrations.

In addition, the Bode diagrams indicate the existence of three main regions. The first one at low frequencies, *i.e.*, the frequency $f \rightarrow 0$ and the second region at high frequencies in the absence and presence of different concentrations of MB-C₂-MB and MB-C₈-MB, *i.e.*, $f \rightarrow \infty$. In these regions, the modulus of impedance $|Z|$ is practically unaffected by the frequency along with the phase angle ϕ ($\phi \rightarrow 0$) and imaginary component $(-Im(Z) \rightarrow 0)$ go both to zero. Thus, these two regions have a typical ohmic behavior where the measured impedances correspond respectively to the polarization resistance ($f \rightarrow 0$) and the electrolyte resistance ($f \rightarrow \infty$) [4].

However, the third region corresponding to the intermediate frequencies shows a linear dependence of $\log|Z| - \log f$ with a slope $(\partial \log|Z|)/(\partial \log f)$ lower than the opposite of unity (-1), and an optimal phase angle ϕ more than -90° . This result is often misinterpreted in the literature [4, 17, 18] in terms of surface heterogeneities, as well as the non-ideal character of the capacitive process governing the electrochemical interface. Indeed, this observation can now be recorded even though the capacitive behavior is purely ideal. This is, in fact, a simple effect of the presence of a non-negligible electrolyte resistance which masks the ideal and non-ideal capacitive behavior (CPE, cf. hereafter) of the kinetically fast step observed at HF.

Linear fitting of data, free from measurement artifact, from the curve ($\log|-Im(Z)|$ vs. $\log f$), insensitive to electrolyte resistance, (Figures 6{d} and 7{d}), to HF, spread over the frequency range [1 kHz–10 kHz], allows us to identify the ideal or non-ideal character of the capacitive behavior of the interface by reference to the slope of the regression line (opposite of CPE exponent) [41]. In the present work, the slope found is greater than the opposite of unity at all the concentrations explored for the two studied inhibitors, as well as for the reference solution. This confirms the non-ideal capacitive behavior of the kinetically fast step observed at HF.

At the end of the apparent frequency segmentation on the Bode representation, the ohmic behavior at high frequencies is clearly broader for the control than in the presence of MB-C₂-MB, and even less in the presence of MB-C₈-MB. In fact, the modulus of impedance $|Z|$ remains virtually stable over circa two decades for the uninhibited solution and MB-C₂-MB, whereas it reduces over less than half a decade for MB-C₈-MB. Furthermore, at low frequencies, *i.e.*, $|Z|_{f \rightarrow 0} = R_s + R_p$ increases with increasing MB-C_{*n*}-MB inhibitor concentration (*n* = 2 and 8), indicating an improvement in inhibiting efficiency up to the concentration of 10^{−3} M. This result, observed in the Bode representation, is as harmonious with the difference in intercepts at HF and LF, respectively, as it is with increasing concentration in the Nyquist representation.

In the light of the above, to understand the interfacial mechanism and gain access to the various electrochemical parameters describing the overall corrosion process in the absence and presence of the inhibitors under study, we have resorted to fitting the impedance spectra with an equivalent electrical circuit to model the interfacial phenomena involved. Each of the components used, connected in series or parallel, are linked to a particular physical phenomenon [41, 42].

3.3.2. Equivalent electrical circuits of the mild steel/HCl 1 M interface

The use of equivalent electrical circuits (EECs) to model each of the elementary steps in the overall corrosion process is becoming increasingly widespread; to extract the parameters needed to understand the system under study [42]. Indeed, several models have been proposed in the literature for the analysis of impedance diagrams relating to the corrosion of steels in acidic media [41]. The simplest approach corresponds to a pure charge transfer reaction on the working electrode, whose circuit is made up of three elements: R_s reflecting the electrolyte resistance, in series with the parallel association of R_{ct} reflecting the charges transfer resistance, and C_{dl} is representing the electrochemical double-layer capacitance. The Nyquist diagram associated with this circuit is a perfect semicircle, which is not practically verified for almost all impedance measurements at electrode/electrolyte interfaces in the case of steel corrosion in acidic media. This classical model approach is suitable for homogeneous systems and cannot be applied to heterogeneous systems. In view of this, the use of a constant-phase element, CPE (Q, n), in place of an ideal capacitor is essential in equivalent electrical circuits when fitting electrochemical impedance diagrams to account for surface inhomogeneity via the coefficient *n* (between 0 and 1) and consequently frequency

dispersion in the dielectric. Indeed, the CPE used to replace the double-layer capacity for a more laborious adjustment is calculated as follows, Equation 14 [42]:

$$Z_{\text{CPE}} = Q^{-1}(j \times \omega)^{-n} \quad (14)$$

where Q is a proportional factor (in $\mu\text{F} \cdot \text{s}^{n-1} \cdot \text{cm}^{-2}$), j is an imaginary number with $j^2 = -1$, n is an exponent related to the phase shift and can be used as a measure of surface heterogeneity and ω is the angular frequency in rad s^{-1} ($\omega_{\text{max}} = 2\pi f_{\text{max}}$, f_{max} is the maximum frequency at which the imaginary component of the impedance is maximum).

The impedance diagrams in the Nyquist, Bode and Betova planes for Q235-steel, immersed in 1 M HCl medium, in the presence and absence of different concentrations of MB-C₂-MB and MB-C₈-MB, in order to extract the parameters necessary for understanding the studied system, were modeled using the following three circuits. Circuits with a single time constant of Randles type $R_s + C_1/R_1$ and modified Randles $R_s + \text{CPE}_1/R_1$ and the circuit with two-time constants $R_s + \text{CPE}_1/[R_1 + \text{CPE}_2/R_2]$ are reported in Figure 8. It's worth pointing out that many researchers use polarization resistance instead of charge transfer resistance in the first two circuits, given the increase in sludge size resulting from the adsorption of inhibitors onto the metal surface [17, 25, 27].

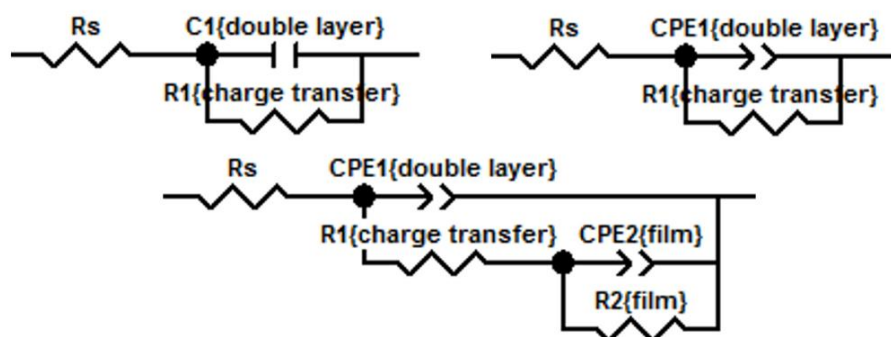
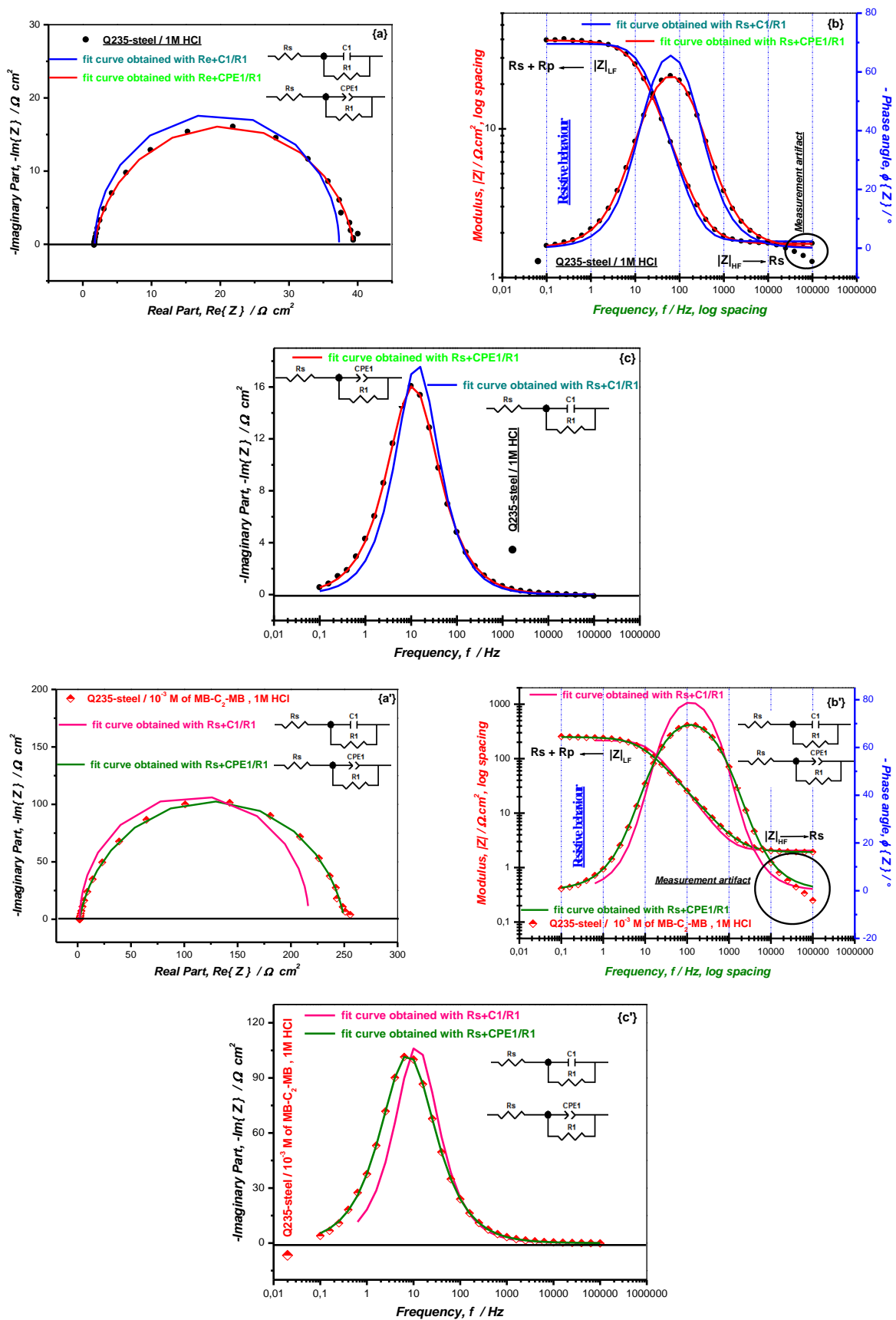


Figure 8. Equivalent electrical circuits proposed to model the behavior of Q235-steel in the presence and absence of different inhibitor concentrations in 1 M HCl medium.

Impedance spectra were fitted, and electrochemical parameters extracted using Z-View software. The algorithm designed for this software package enables impedance spectra to be fine-tuned. The algorithm seeks to minimize the error difference between the experimental data and a mathematical function determined by the equivalent electrical circuit. The difference between the experimental data and the refined data is estimated by an error factor expressed by Equation 15 as follows:

$$\chi'^2 = \sum_{i=1}^n \frac{\left| (Z_{\text{meas}}(i) - Z_{\text{model}}(f_i, \text{param})) \right|^2}{D_i^2} \quad (15)$$

where $Z_{\text{meas}}(i)$ is the impedance measured at frequency f_i . $Z_{\text{model}}(f_i, \text{param})$ is a function of the chosen model, f is the frequency, param is the model parameter (R_s , R_{ct} , $Q_{\text{dl}} \dots$) and D_i is the standard deviation.



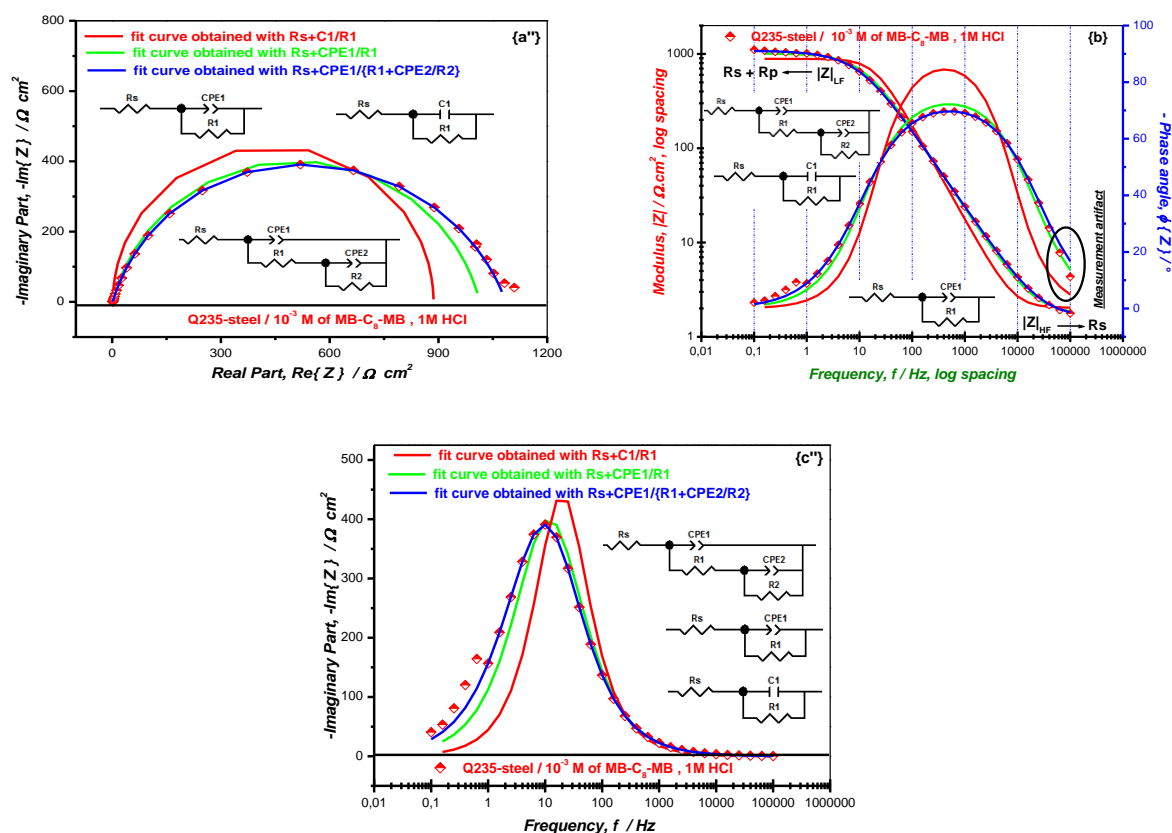


Figure 9. Examples of Nyquist, Bode and Betova representations of experimental and fitted data for Q235-steel in 1 M HCl in the absence (a, b, c) and in the presence of MB-C₂-MB (a', b', c') and MB-C₈-MB (a'', b'', c''), at 10⁻³ M, performed with the Randles electrical circuit, the modified Randles electrical circuit containing the "CPE" and the ladder circuit 2 (R/CPE).

It is clearly found that the impedance spectra of steel in 1 M HCl medium and those in the presence of both inhibitors were very poorly fitted using the classic $R_s + C_{dl}/R_{ct}$ EEC. However, an excellent parametric fit of the experimental impedance spectra in the Nyquist and Bode planes was obtained using the modified Randles model $R_s + (R/CPE)$ in the absence and presence of all MB-C₂-MB concentrations (Figures 6 and 9) and the cascaded $R_s + 2(R/CPE)$ model in the presence of all MB-C₈-MB concentrations (Figures 7 and 9). The experimental and simulated spectra are well correlated with χ^2 coefficient of the order of 10⁻⁴, validating these models.

This confirms that a simple circuit with true capacitance remains inappropriate for modeling the behavior of Q235-steel in a corrosive environment 1 M HCl, and that the CPE is the best way to account for the frequency distribution due to surface heterogeneity. It also confirms that for all MB-C₈-MB concentrations, the electrochemical behavior is different from that of MB-C₂-MB and 1 M HCl, due to the appearance of a second time constant. This second relaxation phenomenon or time constant is generally attributed to the presence of an additional manifest process on the metallic surface. This simple qualitative analysis confirms the formation of a barrier film directly linked to the size of the hydrophobic part of the surfactants.

Impedance parameters R_s , R_{ct} , Q_{dl} , n_1 , R_f , Q_f , n_2 , R_p , χ'^2 recorded from the fitting of diagrams are listed in Table 6. The charge transfer resistance R_{ct} is calculated from the impedance difference between low and high frequencies in the case of 1 M HCl alone and in the presence of different MB-C₂-MB concentrations, *i.e.*, the diameter of the semicircle, while this difference represents the polarization resistance R_p with $R_p = R_{ct} + R_f$ at different MB-C₈-MB concentrations [13]. According to the literature [4, 10, 13, 17, 18], the values of the pseudo-double layer capacity C_{dl} (Equation 16) and the film capacitance C_f (Equation 17) are determined by a transfer function with the constant phase element CPE (Q , n) as follows:

$$C_{dl} = \left(Q_{dl} \times R_{ct}^{1-n_{dl}} \right)^{1/n_{dl}} \quad (16)$$

$$C_f = \left(Q_f \times R_f^{1-n_f} \right)^{1/n_f} \quad (17)$$

Besides, the relaxation constants of the double layer ((Equation 18) and the film (Equation 19) is given by the following equations:

$$\tau_{dl} = R_{ct} \times C_{dl} \quad (18)$$

$$\tau_f = R_f \times C_f \quad (19)$$

According to the literature [27, 43–45], Equations 16–18 are only valid for a simple CPE/R interconnection in the absence of any electrolyte resistance. However, these same equations are now found in various works, which unfortunately distort the interpretation of the interfacial process [4, 10, 17, 18].

It can be assumed that the parameter R_p^{-1} is directly related to the corrosion rate. The inhibition efficiency from the polarization resistance in the presence of different MB-C₈-MB concentrations is calculated according to Equation 20:

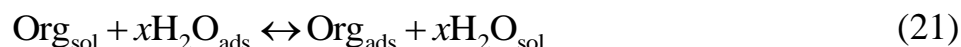
$$\eta_{EIS} \% = \left(1 - \frac{R_p^0}{R_p^{inh}} \right) \times 100 \quad (20)$$

The analysis of the electrochemical parameters illustrated in Table 6 shows that the electrolyte resistance determined between the reference and working electrodes can be obtained from the intersection of the abscissa axis with the semicircle at $f \rightarrow \infty$, $R_s = 2 \Omega \text{ cm}^2$ in all the solutions studied. We also note that the addition of MB-C₂-MB and MB-C₈-MB reduces the CPE parameter value of the double layer Q_{dl} by 588.86 $\mu\text{F s}^{n-1} \text{ cm}^{-2}$ in the corrosive solution alone to 134.89 and 35.28 $\mu\text{F s}^{n-1} \text{ cm}^{-2}$ for MB-C₂-MB and MB-C₈-MB, respectively at the same concentration of 10^{-3} M. On the other hand, we are witnessing an increase in charge transfer resistance of 37.71 $\Omega \cdot \text{cm}^2$ in the absence of an inhibitor at 248.1 and 803.3 $\Omega \cdot \text{cm}^2$ respectively, at 10^{-3} M concentration in MB-C₂-MB and MB-C₈-MB. The changes in Q_{dl} and R_{ct} reflect the decrease in the active surface area of the metal that can be

attributed to the adsorption of the inhibitor molecules on the surface of the steel, thus forming a protective layer [4, 25, 46]. This result is reflected in the increase in inhibition efficiencies. The values of the coefficient n_1 below one confirms the heterogeneity of the surface of the steel studied as explained above [8]. The electrochemical parameters of the film follow the same trend as those of charge transfer and show that the film becomes more and more resistant with the increase in MB-C8-MB content. The inhibiting efficiency reaches a value of 85% at 10^{-3} M for MBC2-MB and 96% at the same concentration for MB-C8-MB.

3.4. Thermodynamic properties of MB-C₈-MB adsorption

The adsorption isotherm provides useful information on the corrosion inhibition mechanism. Determining the relationship between corrosion inhibition and adsorption is therefore of great interest. Adsorption of inhibitor molecules at the Q235-steel/1 M HCl interface takes place by the substitution of water molecules according to Eq. 21 [10]:



Org_{sol} and Org_{ads} are organic molecules in solution and adsorbed on the surface of the Q235-steel, respectively. x is the ratio of the size factor representing the number of water molecules replaced by an organic inhibitor molecule. It is assumed to be independent of the surface coverage rate or electrode charge [10, 23].

Surface coverage ratio values are obtained from dc polarization methods (R_p -Fit) (θ_{PP}) and EIS measurements (θ_{EIS}) at different MB-C₈-MB concentrations and at 298 K according to Equation 22.

$$\theta = \frac{\eta\%}{100} \quad (22)$$

The most commonly used adsorption isotherms are confounded with experimental data, such as Langmuir, Flory-Huggins, Temkin, Frumkin, Freundlich and the El-Awady model. Indeed, electrochemical systems are often referred to as ideal or non-ideal adsorptions due to the different assumptions on which each adsorption isotherm is based. All these isotherms obey a common general expression given below by Equation 23 [10]:

$$f(\theta, x) \exp(-2a\theta) = K_{\text{ads}} \times C_{\text{inh}} \quad (23)$$

where $f(\theta, x)$ is the configurationally factor which depends upon the physical model and the assumptions underlying the derivation of the isotherm; C_{inh} is the inhibitor concentration in the electrolyte; a is the molecular interaction parameter depending on the molecular interactions in the adsorption layer and on the degree of heterogeneity of the surface, and K_{ads} is the equilibrium constant of the adsorption process which is temperature dependent and is related to the free energy of adsorption according to Equation 24.

Table 6. Set of electrochemical parameters of the mild *Q235-steel*/1 M HCl interface obtained in the absence and presence of MB-C₂-MB and MB-C₈-MB at different concentrations and 298 K, after 30 min immersion.

Interface	$R_s=R_\Omega$	1 st time constant			2 nd time constant			R'_p	$\eta_{\text{EIS}}\%$	χ'^2
		$10^6 Q_{\text{dl}}$	$n_{\text{CPE1}}=n_{\text{dl}}$	R_{ct}	$10^3 \cdot Q_{\text{f}}$	$n_{\text{CPE2}}=n_{\text{f}}$	R_{f}			
Q235-steel/1 M HCl	1.685	588.86	0.8998	37.71	–	–	–	37.71	–	0.0036
Q235-steel/ 10^{-6} M of MB-C ₂ -MB, 1 M HCl	1.726	443.97	0.8977	45.12	–	–	–	45.12	16.42	0.0024
Q235-steel/ 10^{-5} M of MB-C ₂ -MB, 1 M HCl	1.822	217.13	0.8852	80.02	–	–	–	80.02	52.87	0.0017
Q235-steel/ 10^{-4} M of MB-C ₂ -MB, 1 M HCl	1.898	151.66	0.8806	202.2	–	–	–	202.20	81.35	0.0015
Q235-steel/ 10^{-3} M of MB-C ₂ -MB, 1 M HCl	1.915	134.89	0.8796	248.1	–	–	–	248.10	84.80	0.0037
Q235-steel/ 10^{-6} M of MB-C ₈ -MB, 1 M HCl	1.921	89.01	0.8783	391.7	675.58	0.8369	98.45	490.15	92.30	0.0012
Q235-steel/ 10^{-5} M of MB-C ₈ -MB, 1 M HCl	2.017	64.07	0.8605	422.3	454.90	0.8032	119.30	541.60	93.03	0.0041
Q235-steel/ 10^{-4} M of MB-C ₈ -MB, 1 M HCl	1.792	47.96	0.8599	620.5	393.30	0.7705	170.20	790.70	95.23	0.0019
Q235-steel/ 10^{-3} M of MB-C ₈ -MB, 1 M HCl	1.587	35.28	0.8342	803.3	279.15	0.7646	280.50	1083.80	96.52	0.0007

* R_Ω , R_{ct} , R_{f} and R_p are given in (Ω , cm²); Q_{dl} and Q_{f} are given in (sⁿ, $\Omega^{-1} \cdot \text{cm}^{-2}$)

$$\Delta_r G_{\text{ads}}^0 = -RT \ln(55.55 \times K_{\text{ads}}) \quad (24)$$

where R is the universal gas constant ($R=8.314 \text{ J} \cdot \text{K}^{-1} \cdot \text{mol}^{-1}$) and T is the thermodynamic temperature (K). In the above equation, $55.5 \text{ mol} \cdot \text{L}^{-1}$ is used for molar concentration of water in solution. Table 7 regroups the conventional and linearized forms used to describe these isotherms.

Table 7. Conventional and linear forms of the most used adsorption isotherm models.

Isotherm	Conventional form	Linearized form
Langmuir	$\frac{\theta}{1-\theta} = K_{\text{ads}} C_{\text{inh}}$	$\frac{C_{\text{inh}}}{\theta} = \frac{1}{K_{\text{ads}}} + C_{\text{inh}}$
El-Awady	$\left(\frac{\theta}{1-\theta}\right)^{1/y} = K_{\text{ads}} C_{\text{inh}}$	$\log\left(\frac{\theta}{1-\theta}\right) = y \log K_{\text{ads}} + y \log C_{\text{inh}}$
Flory–Huggins	$\frac{\theta}{x(1-\theta)^x} = K_{\text{ads}} C_{\text{inh}}$	$\log\left(\frac{\theta}{C_{\text{inh}}}\right) = \ln(x K_{\text{ads}}) + x \log(1-\theta)$
Temkin	$e^{-2a\theta} = K_{\text{ads}} C_{\text{inh}}$	$\theta = -\frac{1}{2a} \ln K_{\text{ads}} - \frac{1}{2a} \ln C_{\text{inh}}$
Frumkin	$\left(\frac{\theta}{1-\theta}\right) e^{-2a\theta} = K_{\text{ads}} C_{\text{inh}}$	$\ln\left(\frac{\theta}{C_{\text{inh}}(1-\theta)}\right) = \ln K_{\text{ads}} + 2a\theta$
Freundlich	$\theta = K_{\text{ads}} (C_{\text{inh}})^n$	$\ln \theta = \ln K_{\text{ads}} + n \ln C_{\text{inh}}$

Figure 10 shows the linear fit according to the two curves derived from electrochemical techniques: polarization curves (R_p -Fit) and electrochemical spectroscopy impedance. Based on these previous methods, the adsorption parameters deduced from the different isotherms and values of the determination coefficient R^2 are recorded in Table 8.

Table 8 shows that the best fit is obtained by using the Langmuir adsorption isotherm with a regression coefficient R^2 of 1 and that the slope of the corresponding equation differs slightly from the unit. Therefore, the Langmuir model is apparently appropriate to describe the adsorption process, as usually indicated by several researchers [10, 23].

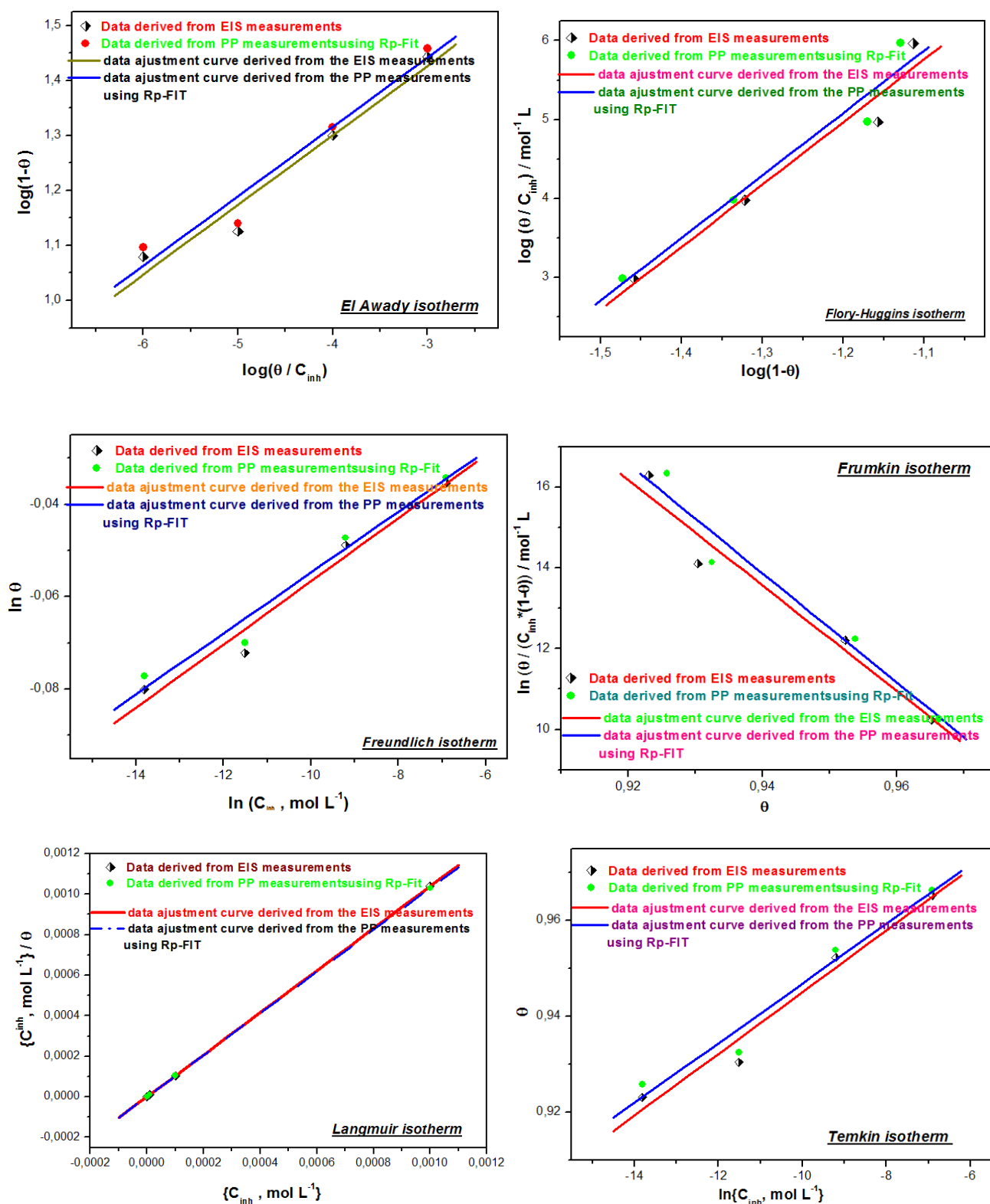


Figure 10. Different adsorption isotherms tested for Q235-steel corrosion in 1 M HCl containing MB-C₈-MB at 298 K.

Table 8. Adsorption parameters deducted from linearizing various adsorption isotherms for Q235-steel corrosion in 1 M HCl in the presence of MB-C₈-MB at 298 K.

Isotherm	Method	R^2	Parameter	K_{ads}	$\Delta_r G_{\text{ads}}^0$
Langmuir	R_p -fit	1	Slope 1.03	1.25×10^6	−46.20
	EIS	1	1.04	2.26×10^6	−47.80
El-Awady	R_p -fit	0.9548	$\frac{1}{y}$ 7.93	2.70×10^{14}	−95.4
	EIS	0.9573	7.90	1.85×10^{14}	−94.4
Flory-Huggins	S&G	0.9532	$\frac{x}{y}$ 7.93	4.99×10^{13}	−91.10
	EIS	0.9557	7.92	3.81×10^{13}	−90.40
Temkin	R_p -fit	0.9657	$\frac{a}{b}$ −80.50	3.65×10^{70}	−426.00
	EIS	0.9684	−77.60	1.20×10^{68}	−412.00
Freundlich	R_p -fit	0.9661	$\frac{a}{b}$ 0.00657	1.01	−10.3
	EIS	0.9689	0.00683	1.01	−10.3
Frumkin	R_p -fit	0.9544	$\frac{a}{b}$ −67.6	1.54×10^{61}	−371.00
	EIS	0.9579	−65.3	1.65×10^{59}	−359.00

However, such deviation may be rooted in Langmuir's assumptions, which are certainly not respected. In fact, Langmuir's model remains hypothetical and often refers to ideal adsorption, which is not appropriate in non-ideal electrochemical systems [23]. This is why, in the present study, we were tempted to look for other models considering the non-ideal character of the adsorption process. Thus, isotherms, El-Awady, Flory–Huggins, Temkin, Frumkin as well as Freundlich, were undertaken. Initially, the coefficients of determination values were very close to unity, prompting us to investigate further.

Indeed, the reciprocal of “y” obtained from the El-Awady isotherm is of the order of 8; approximately equal to the value of the size parameter “x” deduced from the Flory-Huggins isotherm, implying that eight water molecules were replaced by one MB-C₈-MB molecule during the inhibition process. As a result, the adsorbed species are attached to more than one active site on the metal surface, in complete contradiction to Langmuir's hypothesis that the metal surface contains a fixed number of adsorption sites, each containing only one adsorbate-inhibiting molecule. This result suggests that certain functional groups of the

surfactant are adsorbed onto the Q235-steel surface while other parts of the MB-C₈-MB remain free in solution, *i.e.*, only a certain number of segments of the long hydrophobic chain of the surfactant are in direct contact with the metal surface while the tails remain in solution to chase water molecules away from the metal surface. We can therefore conclude that the MB-C₈-MB inhibitor is probably adsorbed vertically to the surface of Q235-steel, while the occurrence of planar adsorption by the MB-C₈-MB compound studied can be ruled out.

On the other hand, the fact that the MB-C₈-MB adsorption process also follows the Temkin and Frumkin isotherms is an indication of the existence of molecular interaction in the adsorbed layer, which is not totally ideal as suggested by the Langmuir isotherm. It is further confirmed by the negative sign of the intermolecular interaction parameter between molecules adsorbed to the metal surface “ a^{Temk} ” and “ a^{Frum} ” respectively, of the Temkin and Frumkin isotherms, indicating lateral interactions in the adsorbed layer.

Table 8 makes this clear; the value of K_{ads} derived from the different isotherms is high, except in the Freundlich isotherm model, which indicates a high adsorption of the MB-C₈-MB inhibitor to the metal surface. The values of K_{ads} and $\Delta_r G_{\text{ads}}^0$ obtained by the Freundlich adsorption isotherm are very low, thus making the applicability of this isotherm to the system questionable. Indeed, the “ a^{freund} ” value of the Freundlich isotherm is far from the typical value of 0.6 [10], which means that the adsorption process studied cannot reasonably be modeled by the Freundlich isotherm, even though the value of R^2 which appears to be good obtained from the corresponding plot.

Finally, the standard Gibbs energy is evaluated from Equation 24. Researchers [10, 17, 23, 25, 46] calculate and discuss this variable on the basis of values of around $-20 \text{ kJ}\cdot\text{mol}^{-1}$ or less negative are linked to an electrostatic interaction between charged organic molecules and the charged Q235-steel surface, physisorption; those of $-40 \text{ kJ}\cdot\text{mol}^{-1}$ or more negative involve charge sharing or the transfer of organic molecules onto Q235-steel surface to form a coordination bond, *i.e.* chemisorption [8]. In the Langmuir model, the energy values approach $-40 \text{ kJ}\cdot\text{mol}^{-1}$, in favor of chemisorption process. It is therefore not easy to distinguish between physisorption and chemisorption simply based on these criteria, especially when charged species are adsorbed. The possibility of Columbic interactions between adsorbed anions and specifically adsorbed cations can increase the Gibbs energy even if no chemical bonding occurs [10]. The inhibition process, in a real system, remains complex and poorly understood. This means that one or all the above mechanisms may be at work.

3.5. Effect of surfactant hydrophobic chain length on inhibition efficiency

In this section, we present only the results obtained by electrochemical impedance spectroscopy of Q235-steel in 1 M HCl in the absence and presence of MB-C₂-MB, MB-C₄-MB, MB-C₆-MB, MB-C₈-MB and MB-C₁₀-MB, at the optimum concentration of 10^{-3} M . The aim of this study was to investigate the effect of surfactant hydrophobicity on inhibiting efficiency. Nyquist, Bode and Betova diagrams of Q235-steel immersed in 1 M HCl without

and with addition of MB- C_n -MB surfactants such that $n = 2, 4, 6, 8, 10$ are shown in Figure 11. The data represented in these diagrams are obtained after 30 min of immersion in the open circuit and at 298 K. Table 9 shows the various parameters resulting from the adjustment of electrochemical impedance data using the two EEC with one and two-time constants.

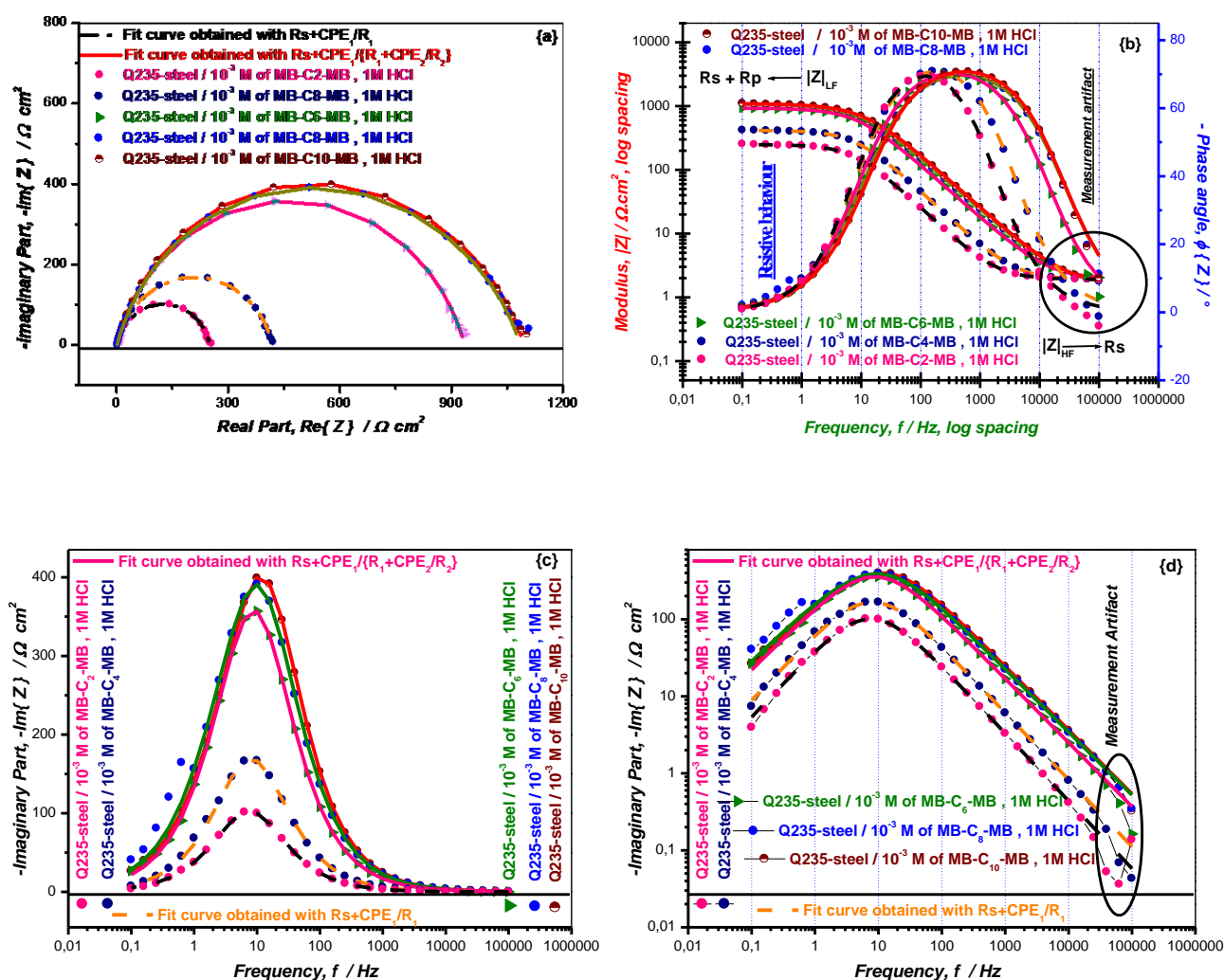


Figure 11. Nyquist {a}, Bode {b}, and Betova {c and d} diagrams for mild Q235-steel in 1 M HCl at 10^{-3} M concentration of (MB- C_n -MB) with $n = 2, 4, 6, 8$ & 10 after 30 min of immersion at the open circuit potential and at 298 K.

The values of the electrochemical parameters resulting from the parametric fitting using the modified Randles circuit has a single time constant for hydrophobic short chain surfactants with $n = 2, 4$ and two-time constant in cascade circuit for long chain surfactants with $n = 6, 8$ & 10. Besides, inhibiting efficiency $\eta\%$ for a concentration of 10^{-3} M in MB- C_n -MB are combined in Table 9. These efficiencies are calculated from R_p values according to Equation 13.

Table 9. Electrochemical parameter sets of Q-235-steel/1 M HCl interface obtained in the absence and presence of MB-C₂-MB, MB-C₄-MB, MB-C₆-MB, MB-C₈-MB and MB-C₁₀-MB at the optimum concentration of 10^{−3} M and 298 K, after 30 min of immersion.

Interface	1 st time constant				2 nd time constant			R'_p	$\eta_{\text{EIS}}\%$	χ'^2
	R_Ω	$10^6 \cdot Q_{\text{dl}}$	$n_{\text{CPE1}}=n_{\text{dl}}$	R_{ct}	$10^3 \cdot Q_{\text{f}}$	$n_{\text{CPE2}}=n_{\text{f}}$	R_{f}			
Q235-steel/1 M HCl	1.685	588.86	0.8998	37.71	—	—	—	37.71	—	0.0036
Q235-steel/10 ^{−3} M of MB-C ₂ -MB, 1 M HCl	1.915	134.89	0.8796	248.1	—	—	—	248.1	84.80	0.0035
Q235-steel/10 ^{−3} M of MB-C ₄ -MB, 1 M HCl	1.891	78.99	0.8705	416.0	—	—	—	416.0	90.93	0.0087
Q235-steel/10 ^{−3} M of MB-C ₆ -MB, 1 M HCl	1.931	41.98	0.8531	741.6	300.00	0.7701	191.8	933.4	95.95	0.0019
Q235-steel/10 ^{−3} M of MB-C ₈ -MB, 1 M HCl	1.587	35.28	0.8342	803.3	279.15	0.7646	280.5	1083.8	96.52	0.0007
Q235-steel/10 ^{−3} M of MB-C ₁₀ -MB, 1 M HCl	1.659	28.19	0.8513	811.2	260.40	0.7595	283.1	1094.3	96.55	0.0041

* R_Ω , R_{ct} , R_{f} and R_p are given in ($\Omega \cdot \text{cm}^2$); Q_{dl} and Q_{f} are given in ($\text{s}^n, \Omega^{-1} \cdot \text{cm}^{-2}$).

The results in Table 9 show that by increasing the length of the hydrophobic chain, the effectiveness of inhibition increases. This behavior can be attributed to the presence of these chains which form successive protective layers onto the metal surface, keeping corrosive species away from the metal surface and reducing the corrosion process. Hence, by increasing the length of the hydrophobic chain, the adsorption rate improves on Q235-steel, due to the amphipathic structure of the surfactant inhibitors, and consequently the increase of inhibition efficiency.

Conclusion

The bis-mercapto-benzimidazoles studied (MB-C_n-MB with $n = 2, 4, 6, 8$ & 10) showed excellent inhibition performance against corrosion of mild Q235-steel in molar hydrochloric acid. Inhibition efficiencies, estimated by various experimental techniques (PP and EIS) follow the same trend when varying the concentration of MB-C₂-MB and MB-C₈-MB inhibitors.

Potentiodynamic polarization curves (PP) were exploited differently depending on the potential window explored. These are the Tafel-fit, Stern-fit and R_p -fit models. Current densities derived from Tafel-fit were found to be significantly higher than those derived from the other methods. Such a difference was attributed to the effect of high electrode polarization recorded at high overvoltage. Indeed, recording $i-E$ curves over a wide potential range can lead to irreversible changes to the metal surface. As a result, it is not always possible to accurately determine corrosion current densities, in a real condition, using Tafel-fit where these currents are often poorly estimated. It should also be pointed out that the Tafel slopes of the cathodic branch of each polarization curve differ from those estimated by the non-linear fit in the pre-Tafelian region using the Stern model, where excessive electrode polarization is completely avoided.

On the other hand, electrochemical impedance diagrams were investigated in three representation planes (Nyquist, Bode and Betoova). Graphical analysis claims the existence of a single time constant. However, the electrical circuit equivalent to two-time constants was the most suitable for fitting the MB-C₈-MB data to all concentrations, whereas for MB-C₂-MB, a CEE with a single constant was sufficient to faithfully reproduce the impedance data. It should be noted that the first time constant is related to the faradic process that takes place parallel to the double-layer phenomenon, while the second time constant relates the strong adsorption of the inhibitor MB-C₈-MB to the metal surface compared to its counterpart MB-C₂-MB.

In addition, in order to better understand the adsorption process, six isotherm models were listed at one or more adsorption sites with or without possible interactions between inhibitor and metal surface. The Langmuir model, although a good fit to the experimental data, can in no way reproduce the actual state of corrosion because of the multiple assumptions governing the model, which often refers to ideal adsorption, which runs counter to adsorption in non-ideal systems. On the other hand, with the exception of the Freundlich

model, the other models studied respond correctly to the experimental data with very acceptable statistical parameters.

The impedance results obtained also reveal an increase in protective power as the hydrophobic chain length of the inhibitors increases, with the estimated inhibiting efficiencies for a 30 min immersion time evolving in the order MB-C₁₀-MB (97%) ≥ MB-C₈-MB (97%) ≥ MB-C₆-MB (96%) ≥ MB-C₄-MB (91%) ≥ MB-C₂-MB (85%), indicating that inhibitory properties increase with increasing hydrophobic chain length.

References

1. L. Huang, S.-S. Wang, H.-J. Li, J.-Y. Wang, Z.-G. Li and Y.-C. Wu, Highly effective Q235 steel corrosion inhibition in 1 M HCl solution by novel green strictosamide from *Uncaria laevigata*: Experimental and theoretical approaches, *J. Environ. Chem. Eng.*, 2022, **10**, no. 3, 107581. doi: [10.1016/j.jece.2022.107581](https://doi.org/10.1016/j.jece.2022.107581)
2. L. Li, X. Zhang, J. Lei, J. He, S. Zhang and F. Pan, Adsorption and corrosion inhibition of *Osmanthus fragran* leaves extract on carbon steel, *Corros. Sci.*, 2012, **63**, 82–90. doi: [10.1016/j.corsci.2012.05.026](https://doi.org/10.1016/j.corsci.2012.05.026)
3. X. Li, Y. Ye, T. Liu, W. Zheng, F. Yang, Ha. Zhao and L. Wang, Corrosion inhibition of Q235 steel in 1 M HCl using quaternized tetraaniline as a corrosion inhibitor, *Surf. Topogr.: Metrol. Prop.*, 2017, **5**, 044001. doi: [10.1088/2051-672X/aa8c0e](https://doi.org/10.1088/2051-672X/aa8c0e)
4. M. Beniken, M. Driouch, M. Sfaira, B. Hammouti, M. Ebn Touhami and M.A. Mohsin, Anticorrosion Activity of a Polyacrylamide with High Molecular Weight on C-Steel in Acidic Media: Part 1, *J. Bio Tribo Corros.*, 2018, **4**, no. 38. doi: [10.1007/s40735-018-0155-y](https://doi.org/10.1007/s40735-018-0155-y)
5. E.H. El Assiri, M. Driouch, J. Lazrak, Z. Bensouda, A. Elhaloui, M. Sfaira, T. Saffaj and M. Taleb, Development and validation of QSPR models for corrosion inhibition of carbon steel by some pyridazine derivatives in acidic medium, *Heliyon*, 2020, **6**, no. 10, E05067. doi: [10.1016/j.heliyon.2020.e05067](https://doi.org/10.1016/j.heliyon.2020.e05067)
6. R. Solmaz, Investigation of the inhibition effect of 5-((E)-4-phenylbuta-1,3-dienylideneamino)-1,3,4-thiadiazole-2-thiol Schiff base on mild steel corrosion in hydrochloric acid, *Corros. Sci.*, 2010, **52**, no. 10, 3321–3330. doi: [10.1016/j.corsci.2010.06.001](https://doi.org/10.1016/j.corsci.2010.06.001)
7. N. Achnine, M. Driouch, A. Elhaloui, Z. Lakbaibi, E.H. El Assiri, M. Kadiri, M. Sfaira, O. Dagdag, A. Berisha, B. El Ibrahim, S. Kaya, L. Guo and A. Zarrouk, A critical view of computational chemistry methods in understanding corrosion inhibition of 6-chloro-2-phenylimidazo[1,2-*b*]pyridazine in 1 M and 5 M HCl, *International Int. J. Corros. Scale Inhib.*, 2023, **12**, no. 3, 888–912. doi: [10.17675/2305-6894-2023-12-3-6](https://doi.org/10.17675/2305-6894-2023-12-3-6)
8. R. Solmaz, Investigation of adsorption and corrosion inhibition of mild steel in hydrochloric acid solution by 5-(4-Dimethylaminobenzylidene)rhodanine, *Corros. Sci.*, 2014, **79**, 169–176. doi: [10.1016/j.corsci.2013.11.001](https://doi.org/10.1016/j.corsci.2013.11.001)

-
9. F. Bentiss, M. Outirite, M. Traisnel, H. Vezin, M. Lagrenée, B. Hammouti, S.S. Al-Deyab and C. Jama, Improvement of corrosion resistance of carbon steel in hydrochloric acid medium by 3,6-bis(3-pyridyl)pyridazines, *Int. J. Electrochem. Sci.*, 2012, **7**, 1699–1723.
 10. M. Beniken, M. Driouch, M. Sfaira, B. Hammouti, M. Ebn Touhami and M.A. Mohsin, Kinetic–Thermodynamic Properties of a Polyacrylamide on Corrosion Inhibition for C-Steel in 1.0 M HCl Medium: Part 2, *J. Bio Tribo Corros.*, 2018, **4**, no. 34. doi: [10.1007/s40735-018-0152-1](https://doi.org/10.1007/s40735-018-0152-1)
 11. Z. Bensouda, M. Driouch, R.A. Belakhmima, M. Sfaira, M. Ebn Touhami and A. Farah, Thymus Sahraouian Essential Oil as Corrosion Eco-friendly Inhibitor for Mild Steel in a Molar Hydrochloric Acid Solution, *Port. Electrochim. Acta*, 2018, **36**, no. 5, 339–364. doi: [10.4152/pea.201805339](https://doi.org/10.4152/pea.201805339)
 12. Z. Bensouda, M. Driouch, M. Sfaira, A. Farah, M. Ebn Touhami, B. Hammouti and K.M. Emran, Effect of *Mentha Piperita* essential oil on mild steel corrosion in hydrochloric acid, *Int. J. Electrochem. Sci.*, 2018, **13**, 8198–8221. doi: [10.20964/2018.08.79](https://doi.org/10.20964/2018.08.79)
 13. S. Aourabi, M. Driouch, M. Kadiri, F. Mahjoubi, M. Sfaira, B. Hammouti and K.M. Emran, Valorization of *Zea mays* hairs waste extracts for antioxidant and anticorrosive activity of mild steel in 1 M HCl environment, *Arabian J. Chem.*, 2020, **13**, no. 9, 7183–7198. doi: [10.1016/j.arabjc.2020.08.001](https://doi.org/10.1016/j.arabjc.2020.08.001)
 14. E.H. El Assiri, M. Driouch, Z. Bensouda, F. Jhilal, T. Saffaj, M. Sfaira and Y. Abboud, Quantum chemical and QSPR studies of bis-benzimidazole derivatives as corrosion inhibitors by using electronic and lipophilic descriptors, *Desalin. Water Treat.*, 2018, **111**, 208–225. doi: [10.5004/dwt.2018.22198](https://doi.org/10.5004/dwt.2018.22198)
 15. A. Khormali and S. Ahmadi, Experimental and modeling analysis on the performance of 2 mercaptobenzimidazole corrosion inhibitor in hydrochloric acid solution during acidizing in the petroleum industry, *J. Pet. Explor. Prod. Technol.*, 2023, **13**, 2217–2235. doi: [10.1007/s13202-023-01675-6](https://doi.org/10.1007/s13202-023-01675-6)
 16. L. Wang, Evaluation of 2-mercaptobenzimidazole as corrosion inhibitor for mild steel in phosphoric acid, *Corros. Sci.*, 2001, **43**, no. 12, 2281–2289. doi: [10.1016/S0010-938X\(01\)00036-1](https://doi.org/10.1016/S0010-938X(01)00036-1)
 17. M. Damej, S. Kaya, B. EL Ibrahimi, H-S. Lee, A. Molhi, G. Serdaroğlu, M. Benmessaoud, I.H. Ali, S. EL Hajjaji and H. Lgaz, The corrosion inhibition and adsorption behavior of mercaptobenzimidazole and bis-mercaptobenzimidazole on carbon steel in 1.0M HCl: Experimental and computational insights, *Surf. Interfaces*, 2021, **24**, 101095. doi: [10.1016/j.surfin.2021.101095](https://doi.org/10.1016/j.surfin.2021.101095)
 18. M. Damej, M. Benmessaoud, S. Zehra, S. Kaya, H. Lgaz, A. Molhi, N. Labjar, S. El Hajjaji, A.A. Alrashdi and H.-S. Lee, Experimental and theoretical explorations of S-alkylated mercaptobenzimidazole derivatives for use as corrosion inhibitors for carbon steel in HCl, *J. Mol. Liq.*, 2021, **331**, 115708. doi: [10.1016/j.molliq.2021.115708](https://doi.org/10.1016/j.molliq.2021.115708)

-
19. O.P. Suri, R.K. Khajuria, D.B. Saxena, N.S. Rawat and C.K. Synthesis and spectral studies of 2-mercapto-benzimidazole derivatives. II, *J. Heterocycl. Chem.*, 1983, **20**, no. 3, 813–814. doi: [10.1002/jhet.5570200363](https://doi.org/10.1002/jhet.5570200363)
 20. R. Zniber, A. Moussaif, R. Achour and M. El Ghoul, Préparation de macromolécules dérivées du benimidazole, *Ann. Pharm. Fr.*, 2002, **60**, no. 5, 345–347. doi: [APF-09-2002-60-5-0003-4509-101019-ART10](https://doi.org/APF-09-2002-60-5-0003-4509-101019-ART10)
 21. F. Mansfeld, Tafel slopes and corrosion rates obtained in the pre-Tafel region of polarization curves, *Corros. Sci.*, 2005, **47**, no. 12, 3178–3186. doi: [10.1016/j.corsci.2005.04.012](https://doi.org/10.1016/j.corsci.2005.04.012)
 22. F. Mansfeld, Fundamental aspects of the polarization resistance technique – the early days, *J. Solid State Electrochem.*, 2009, **13**, 515–520. doi: [10.1007/s10008-008-0652-x](https://doi.org/10.1007/s10008-008-0652-x)
 23. S. Aourabi, M. Driouch, M. Sfaira, F. Mahjoubi, B. Hammouti, C. Verma, E.E. Ebenso and L. Guo, Phenolic fraction of Ammi visnaga extract as environmentally friendly antioxidant and corrosion inhibitor for mild steel in acidic medium, *J. Mol. Liq.*, 2021, **323**, 114950. doi: [10.1016/j.molliq.2020.114950](https://doi.org/10.1016/j.molliq.2020.114950)
 24. S. Aourabi, M. Driouch, M. Kadiri, N. Achnine, M. Sfaira and F. Mahjoubi, Synergetic Effect between Phenolic Extracts of *Ammi visnaga* and *Zea mays* Formulation on the Corrosion of Mild Steel in 1 M HCl Solution, *J. Chem.*, 2021, 5589175. doi: [10.1155/2021/5589175](https://doi.org/10.1155/2021/5589175)
 25. M. Idboumlik, M. Kadiri, N. Hamdi, M. Driouch, A.F.I. Ngopoh, I. Lakkab, E.-E. Bendeif, M. Sfaira, B. El Bali, M. Lachkar and A. Zarrouk, Synthesis of novel hybrid decavanadate material $(\text{NH}_4)_2(\text{H}_2\text{en})_2\{\text{V}_{10}\text{O}_{28}\} \cdot 4\text{H}_2\text{O}$: Characterization, anticorrosion and biological activities, *Mater. Chem. Phys.*, 2022, **287**, 126211. doi: [10.1016/j.matchemphys.2022.126211](https://doi.org/10.1016/j.matchemphys.2022.126211)
 26. A. Kosari, M. Momeni, R. Parvizi, M. Zakeri, M.H. Moayed, A. Davoodi and H. Eshghi, Theoretical and electrochemical assessment of inhibitive behavior of some thiophenol derivatives on mild steel in HCl, *Corros. Sci.*, 2011, **53**, 3058–3067. doi: [10.1016/j.corsci.2011.05.009](https://doi.org/10.1016/j.corsci.2011.05.009)
 27. W.J. Lorenz and F. Mansfeld, Determination of corrosion rates by electrochemical DC and AC methods, *Corros. Sci.*, 1981, **21**, no. 9–10, 647–672. doi: [10.1016/0010-938X\(81\)90015-9](https://doi.org/10.1016/0010-938X(81)90015-9)
 28. I. Epelboin, M. Keddam and H. Takenouti, Use of impedance measurements for the determination of the instant rate of metal corrosion, *J. Appl. Electrochem.*, 1972, **2**, 71–79. doi: [10.1007/BF00615194](https://doi.org/10.1007/BF00615194)
 29. C. Wagner and W. Traud, The interpretation of corrosion phenomena by superimposition of electrochemical partial reactions and the formation of potentials of mixed electrodes. *Z. Elektrochem.*, 1938, **44**, 391–402.
 30. M. Stern and A.L. Geary, Electrochemical Polarization: I. A Theoretical Analysis of the Shape of Polarization Curves, *J. Electrochem. Soc.*, 1957, **104**, no. 56, 56–63. doi: [10.1149/1.2428496](https://doi.org/10.1149/1.2428496)

-
31. K.F. Bonhoeffer and W. Jena, Über das elektromotorische Verhalten von Eisen, *Z. Elektrochem. Angew. Phys. Chem.*, 1951, **55**, no. 2, 151–154. doi: [10.1002/bbpc.19510550215](https://doi.org/10.1002/bbpc.19510550215)
 32. J.G. Hines, Analysis of Complex Polarisation Curves, *Br. Corros. J.*, 1983, **18**, no. 1, 10–14. doi: [10.1179/000705983798274001](https://doi.org/10.1179/000705983798274001)
 33. H. Bentrach, Y. Rahali and A. Chala, Gum Arabic as an ecofriendly inhibitor for API 5L X42 pipeline steel in HCl medium, *Corros. Sci.*, 2014, **82**, 426–431. doi: [10.1016/j.corsci.2013.12.018](https://doi.org/10.1016/j.corsci.2013.12.018)
 34. N. Soltani, N. Tavakkoli, M. Khayat Kashani, M.R. Jalali and A. Mosavizade, Green approach to corrosion inhibition of 304 stainless steel in hydrochloric acid solution by the extract of *Salvia officinalis* leaves, *Corros. Sci.*, 2012, **62**, 122–135. doi: [10.1016/j.corsci.2012.05.003](https://doi.org/10.1016/j.corsci.2012.05.003)
 35. K.S. Cole and R.H. Cole, Dispersion and Absorption in Dielectrics I. Alternating Current Characteristics, *J. Chem. Phys.*, 1941, **9**, 341–351. doi: [10.1063/1.1750906](https://doi.org/10.1063/1.1750906)
 36. K.S. Cole and R.H. Cole, Dispersion and Absorption in Dielectrics II. Direct Current Characteristics, *J. Chem. Phys.*, 1942, **10**, 98–105. doi: [10.1063/1.1723677](https://doi.org/10.1063/1.1723677)
 37. D.W. Davidson and R.H. Cole, Dielectric Relaxation in Glycerol, Propylene Glycol, and *n*-Propanol, *J. Chem. Phys.*, 1951, **19**, 1484–1490. doi: [10.1063/1.1748105](https://doi.org/10.1063/1.1748105)
 38. F. Bentiss, M. Traisnel, L. Gengembre and M. Lagrenée, A new triazole derivative as inhibitor of the acid corrosion of mild steel: electrochemical studies, weight loss determination, SEM and XPS, *Appl. Surf. Sci.*, 1999, **152**, no. 3–4, 237–249. doi: [10.1016/S0169-4332\(99\)00322-0](https://doi.org/10.1016/S0169-4332(99)00322-0)
 39. F. Bentiss, M. Traisnel and M. Lagrenée, Inhibitor effects of triazole derivatives on corrosion of mild steel in acidic media, *Br. Corros. J.*, 2000, **35**, no. 4, 315–320. doi: [10.1179/000705900101501326](https://doi.org/10.1179/000705900101501326)
 40. F. Mansfeld, M.W. Kendig and S. Tsai, Recording and analysis of AC impedance data for corrosion studies 2 experimental approach and results, *Corrosion*, 1982, **38**, no. 11, 570–580. doi: [10.5006/1.3577304](https://doi.org/10.5006/1.3577304)
 41. M.E. Orazem and B. Tribollet, *Electrochemical Impedance Spectroscopy, 2nd Edition*, Wiley, Hoboken, 2017.
 42. A. Lasia, Electrochemical Impedance Spectroscopy and its Applications, in: *Mod. Aspects Electrochem.*, 2002, **32**. doi: [10.1007/0-306-46916-2_2](https://doi.org/10.1007/0-306-46916-2_2)
 43. H. Shih and F. Mansfeld, A fitting procedure for impedance data of systems with very low corrosion rates, *Corros. Sci.*, 1989, **29**, no. 10, 1235–1240. doi: [10.1016/0010-938X\(89\)90070-X](https://doi.org/10.1016/0010-938X(89)90070-X)
 44. E.H. Akroujai, S. Chetoui, N. Benzbiria, A. Barrahi, A. Chraka, A. Djedouani, S. Chtita, S. Lazar, I. Warad, A. Bellaouchou, M. Assouag and A. Zarrouk, ((E)-1-((4-Fluorophenyl)diazenyl)naphthalen-2-ol as an innovative and efficient corrosion inhibitor for carbon steel in 1 M HCl solution: Electrochemical analysis coupled with electronic/atomic-scale computational simulations, *Int. J. Corros. Scale Inhib.*, 2023, **12**, no. 3, 1102–1135. doi: [10.17675/2305-6894-2023-12-3-18](https://doi.org/10.17675/2305-6894-2023-12-3-18)

-
45. L.E. Tsygankova, A.E. Abramov, A.A. Uryadnikov, T.V. Semenyuk, K.O. Strel'nikova, R.K. Vagapov and O.G. Mikhalkina, Study of the protection of carbon steel with an inhibitory composition in hydrogen sulfide environments by electrochemical methods, *Int. J. Corros. Scale Inhib.*, 2023, **12**, no. 3, 811–824. doi: [10.17675/2305-6894-2023-12-3-1](https://doi.org/10.17675/2305-6894-2023-12-3-1)
46. M.E. Ansar, R. Hsissou, B.E. Ibrahimi, A.A. Addi, A. Molhi, M. Damej, S. El Hajjaji and M. Benmessaoud, Electrochemical and thermodynamic study of the inhibitory effect of triglycidyl ether tripropoxy triazine (TGETPT) on the corrosion of carbon steel E24 in 1 M hydrochloric acid medium, *Int. J. Corros. Scale Inhib.*, 2023, **12**, no. 3, 1065–1087. doi: [10.17675/2305-6894-2023-12-3-16](https://doi.org/10.17675/2305-6894-2023-12-3-16)
47. Z.K. Kuraimid, D.S. Abid and A.A.S. Fouda, Insight into the use of 1,3,5,7-tetrahexyl-1,3,5,7-tetraazaadamantane-1,3,5,7-tetraium bromide as a highly efficient inhibitor for the corrosion of C1018 low-carbon steel in acidic medium: Synthesis, characterization, and electrochemical studies, *Int. J. Corros. Scale Inhib.*, 2023, **12**, no. 3, 1162–1179. doi: [10.17675/2305-6894-2023-12-3-20](https://doi.org/10.17675/2305-6894-2023-12-3-20)

